Search for exotic gravitating objects with gravitational lensing

A Thesis in Physics
by Naoki Tsukamoto

Rikkyo University

Abstract

For investigating gravitational theories, it is important to research exotic matters theoretically and observationally. In this thesis, we investigate two methods with gravitational lensing to detect exotic matter objects, especially the Ellis wormhole which is an example of traversable wormholes of the Morris-Thorne class.

It is well known that, for the lensing by a black hole, an infinite number of Einstein rings are formed by the light rays which wind around the black hole nearly on the photon sphere, which are called relativistic Einstein rings. This is also the case for the lensing by a wormhole.

First, we study the Einstein ring and relativistic Einstein rings for the Schwarzschild black hole and the Ellis wormhole. Given the configuration of the gravitational lensing and the radii of the Einstein ring and relativistic Einstein rings, we can distinguish between a black hole and a wormhole in principle. We conclude that we can detect the relativistic Einstein rings by wormholes which have the radii of the throat $a \simeq 0.5$pc at a galactic center with the distance 10Mpc and which have $a \simeq 10$AU in our galaxy using by the most powerful modern instruments which have the resolution of 10^{-2}arcseconds such as a 10-meter optical-infrared telescope.

Second, we investigate the signed magnification sums of general spherical lens models including the singular isothermal sphere, the Schwarzschild lens and the Ellis wormhole. We show that the signed magnification sums are a very useful tool to distinguish exotic lens objects. Future surveys of lensed quasars will give a strict upper bound of the number density for wormholes or detect wormholes.

We may test the hypotheses of astrophysical wormholes by using the Einstein ring systems and the signed magnification sums in the future.

Acknowledgments

During the preparation of this thesis, I have been greatly aided by a lot of people at Rikkyo University. I would like to appreciate my supervisor, Tomohiro Harada, for useful encouragements, discussions and criticisms. I have learned a lot from his sincere efforts for gravitational physics.

I thank my collaborators, Chul-Moon Yoo and Kohji Yajima. I truly feel grateful to Umpei Miyamoto. He has kept to encourage me to investigate my work and to give me valuable advices.

I wish to thank Tsutomu Kobayashi, Shingo Kameda, Noriaki Shibazaki, Hidekazu Tanaka, Shigeaki Yahikozawa, Motoyuki Saijo, Hideki Maeda, Shunji Kitamoto, Hiroshi Murakami, Kentaro Yaji, Tsunehide Kuroki, Tohru Eguchi, Tsuyoshi Houri, Tetsuji Kimura, Masahiro Shimano, Hiroya Nemoto, Satoshi Okuda, Syo Kamata and Kumiko Inagawa for their various helps. I also love to express my appreciation to many other people who cheerfully set the mood for theoretical physics group at Rikkyo University.

I would like to appreciate Fumio Abe, Hideki Asada, Ryuichi Takahashi, Takao Kitamura, Koki Nakajima, Kei Yamada, Toshifumi Futamase, Sasaki Misao, Kenichi Nakao, Masato Nozawa and Masashi Kimura. They gave valuable comments for my work and kindly responded my some rude questions.

My work was supported in part by Rikkyo University Special Fund for Research.

Finally I would like to thank my family for its support.

Contents

Chapter 1

Introduction

General relativity is the simplest gravitational theory which passes the classical tests that are the deflection of light, the time-delay of light and the perihelion shift of mercury [1]. While general relativity has won the confidence of physicists and astronomers, alternative theories have been investigated eagerly because of the possibility of renormalization, an explanation for the rotation curves of galaxies, dark energy and so on.

It is well known that our universe would be filled with dark matter and dark energy. Planck measurements of the cosmic microwave background and the baryon acoustic oscillation show the equation of state for the dark energy $w \equiv p/\rho = -1.13 + 0.13 - 0.10$ (68% C.L.), where p and ρ are the pressure and the energy density, respectively [2]. This implies that exotic matters with $w < -1$ may not be exotic in our universe. For investigating gravitational theories, it is important to research exotic matters theoretically and observationally.

These something dark and exotic can be detected with gravitational lensing effects indirectly. In this thesis, we will investigate the two methods to detect the exotic lens objects with the Einstein gravity. Especially we will research gravitational lensing by a wormhole which is a hypothetical object which connects two or more asymptotic region.

1.1 Gravitational lens

According to legend, when Galilei researched celestial objects with his telescope, a man rejected to use telescopes because he thought that they would be evil tools. This legend teaches us an important lesson that we must understand tools.

Gravitational lensing is a very useful tool for astrophysics and cosmology.

Using the gravitational lensing, we determine the cosmological constant, the distribution of dark matter and the Hubble constant, the existence of extrasolar planets and so on (see Schneider *et al.* [3] and Perlick [4, 5] and Petters *et al.* [6] for the detail of the gravitational lens, and references therein).

Mass lens systems in the weak field have been mainly investigated since gravitational lensing was predicted about one hundred years ago. However, curved spacetimes such as wormhole spacetimes also cause gravitational lens effects (see Visser [7] for the details of the wormholes). Since gravitational lensing of the wormholes was pioneered by Kim and Cho [8] and Cramer *et al.* [9], many interesting aspects of gravitational lensing by various wormholes have been investigated [10, 11, 12, 13, 14, 15, 16]. We may test some hypotheses of astrophysical wormholes by using the gravitational lensing in the future [17, 18, 19, 20].

Darwin studied the orbits of particles and light rays on the Schwarzschild spacetime [21, 22] and he found the relativistic images which are a series of faint images lying just outside the photon sphere [21]. For the past decade, gravitational lensing in the strong gravitational field has been studied eagerly (see Virbhadra and Keeton [23], Virbhadra [24], Bozza [25], Bozza and Mancini [26] and references therein). Frittelli *et al.* [27], Virbhadra and Ellis [28, 29] and Bozza *et al.* [30] studied the gravitational lensing in the strong field with the Schwarzschild spacetime and found infinite images, which are too close to each other to separately resolve. In this thesis, we call these images relativistic images. The gravitational lensing in the strong field on the spherically symmetric static spacetime was investigated by Bozza [31], Hasse and Perlick [32] and Perlick [33]. They showed that the relativistic images are formed not only in the Schwarzschild spacetime but also in the other spherically symmetric static spacetime.

Gravitational lensing is not only important for astrophysics but also interesting as the subject of mathematical physics. Witt and Mao investigated the magnifications for lensing by double lenses and found that the signed magnification sums of the five images become unity inside a caustic [34]. Rhie gave another proof for the invariance of the signed magnification sums of gravitational lensing by double lenses and applied it to the n-point lens systems [35]. The signed magnification sums of the simple galaxy models which are variations on the singular isothermal sphere were studied by Dalal [36], and those of quadruple lenses were investigated by Witt and Mao [37]. Dalal and Rabin showed that residue integrals provide a simple explanation for the invariance of the signed magnification sums [38]. See also Petters *et al.* [6] for the details of the application of the singularity theory to the gravitational lenses. Recently, Werner showed that the signed magnification invariant is a topological invariant [39]. The local magnification relations with a subset of the total number of lensed images have been investigated eagerly [40, 41, 42, 43, 44, 45].

Gravitational lensing may become important to test some gravitational theories. The gravitational lens effects of the braneworld gravity models also have been investigated. Majumdar and Mukherjee [46] and Eiroa [47] studied the gravitational lens effects on a braneworld model. Keeton and Petters studied the gravitational lens effects of the Garriga-Tanaka metric in the type II Randall-Sundrum braneworld gravity model [48].

In this thesis, we will show that the signed magnification sum would be a powerful tool to research the lens objects as well as the total magnification and the magnification ratio if we observe a double image. Over than a hundred Multiple images including double images have been observed so far [49]. Large Synoptic Survey Telescope [50] will find about 8000 multiple images of lensed quasars [51]. The future surveys will give a strict upper bound of the number density for wormholes or detect wormholes.

We will also consider the Einstein ring and relativistic Einstein rings in the Ellis wormhole spacetime and the Schwarzschild spacetime, both of which are static and spherically symmetric ones. We ask whether we can distinguish the Einstein ring systems on the Schwarzschild spacetime and on the Ellis wormhole spacetime? To answer this question, we focus on the relations between the Einstein ring and the relativistic Einstein rings.

1.2 Outline of this thesis

This thesis is organized as follows. In Chapter 2, we introduce the basic equation of gravitational lenses. We review the simple lens equation including the effects of the strong gravitational field in Section 2.1 and the deflection angle of the light ray and the magnification under the weak field approximation in the Schwarzschild spacetime in Section 2.2. In Chapter 3, we review the Morris-Thorne wormhole and the Ellis spacetime and the deflection angle of the light in the Ellis wormhole spacetime. In Chapter 4, we will investigate the gravitational lenses in the weak field limit. We discuss the signed magnification sums of general spherical lens models including the singular isothermal sphere, the Schwarzschild lens and the Ellis wormhole. We will number the real solutions of the lens equation because the signed magnification sums are physical invariants only when all the solutions are real. In Chapter 5, we discuss the gravitational lenses on the spherically symmetric and static spacetime in the strong field limit. In Section 5.1, we review the magnification and the radii of the relativistic images in the strong field limit. In Section 5.2, we discuss the gravitational lensing in the strong field limit on the Schwarzschild spacetime in brief. In Section 5.3, we investigate the gravitational lensing in the strong field limit on the Ellis wormhole spacetime. In Chapter 6, we will investigate two new methods to distinguish between exotic matter objects and black holes with gravitational lenses. In Sec. 6.1, we compare the Einstein ring and the relativistic Einstein rings in the Ellis wormhole spacetime to the ones in the Schwarzschild spacetime and show that we can distinguish between black holes and wormholes. In Sec. 6.2, we show that we can distinguish between mass lenses and exotic matter objects with their signed magnifications. In Chapter 7, we summarize and discuss our result. In Appendix A, we discuss the magnification of the Reissner-Nordstrom Black hole in brief. In Appendix B, we will review the microlensing of exotic lenses in brief. In Appendix C, we will recalculate the deflection angle in the strong field limit in the Ellis wormhole spacetime on the same way as in Bozza's analysis. In this thesis we use the units in which the light speed c and Newton's constant G are unity.

Chapter 2

Basic equations of the gravitational lenses

Mass lens systems in the weak gravitational field have been mainly investigated since gravitational lensing was predicted about one hundred years ago. However, relativists are eager to test the effects of the gravitational lenses in the strong gravitational field because gravitational theories including general relativity have never been tested by any experiments in the strong gravitational field yet.

In this chapter, we will review the basic facts of the gravitational lenses but our treatments for a lens equation and the deflection angle of the light are much less common than traditional ways [3, 6] since we also treat strong gravitational field. In section 2.1, we will introduce an effective deflection angle of the light ray and a lens equation which are not only valid in the weak gravitational field but also in the strong gravitational field. In section 2.2, we review the deflection angle of the light ray in the Schwarzschild spacetime. We will express the deflection angle of the photon with an incomplete elliptic integral of the first kind and the complete elliptic integral of the first kind. In section 2.3, we review the Schwarzschild lens under the weak field approximation [3, 6].

2.1 Lens equation

For the past decade, the lens equations which describe the effects of the strong and weak gravitational field have been investigated [28, 33]. In this thesis, we will use the simplest lens equation [52] since we only consider the cases in weak and strong gravitational field limit.

We will consider the case that both the observer O and the source object

S are far from the lensing object L, or $D_l \gg b$ and $D_{ls} \gg b$, where b is the impact parameter of the photon and D_l and D_{ls} are the separations between the observer and lens and between the lens and source, respectively. The configuration of the gravitational lensing is given in Fig. 2.1. Then, the lens

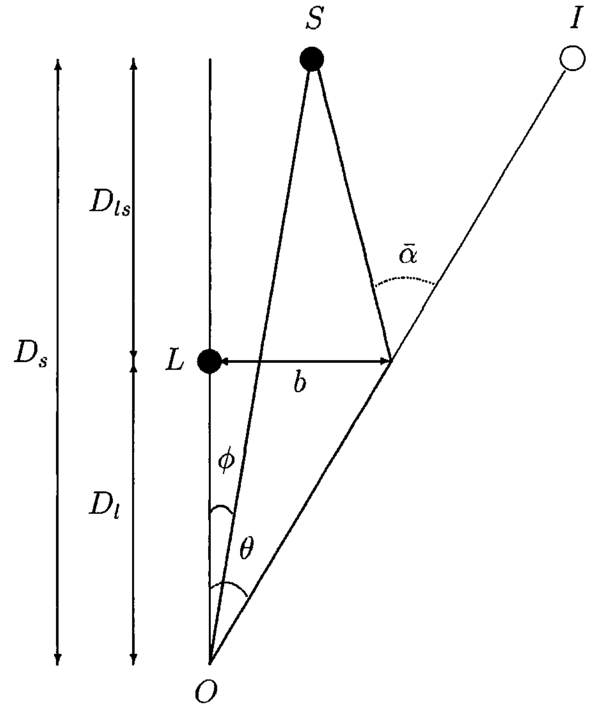

Figure 2.1: The configuration of the gravitational lensing. The light rays emitted by the source S are deflected by the lens L and reach the observer O with the angle of the lensed image θ, instead of the source angle ϕ. b and $\bar{\alpha}$ are the impact parameter and the effective deflection angle, respectively. D_l and D_{ls} are the separations between the observer and the lens and between the lens and the source, respectively. This figure is taken from [52].

equation is given by

$$D_{ls}\bar{\alpha} = D_s(\theta - \phi), \tag{2.1}$$

where $\bar{\alpha} = (\alpha \bmod 2\pi)$ is the effective deflection angle, θ and ϕ are the angles of the lensed image I and the source S to the lens object L from the observer O, respectively, and $D_s = D_l + D_{ls}$ is the separation between the observer O and source S. Note that we have assumed $|\bar{\alpha}| \ll 1$, $|\theta| \ll 1$ and $|\phi| \ll 1$. We have also assume that the light ray bends on the lens plane. This assumption is called the thin lens approximation. The deflection angle can be expressed

$\alpha = \bar{\alpha} + 2\pi n$, where n is a non-negative integer, denoting the winding number of the light ray.

2.2 Deflection angle on the Schwarzschild spacetime

The Schwarzschild spacetime is the static spherically symmetric vacuum solution of the Einstein equations [53]. In this section, we will review the deflection angle on the Schwarzschild spacetime [21, 22, 54, 55] since we have to distinguish exotic lens objects from the Schwarzschild lenses, i.e., mass lenses for detection exotic lens objects. The line element in the Schwarzschild spacetime is given in the following form:

$$ds^2 = -\left(1 - \frac{r_g}{r}\right) dt^2 + \frac{dr^2}{1 - \frac{r_g}{r}} + r^2 d\Omega^2, \tag{2.2}$$

where $d\Omega^2 = d\Theta^2 + \sin^2 \Theta d\Phi^2$ and r_g is the Schwarzschild radius. The spacetime has the Killing vectors $t^\mu \partial_\mu = \partial_t$ and $\phi^\mu \partial_\mu = \partial_\Phi$ for stationarity and axial symmetry.

We can concentrate ourselves on the equatorial plane because of spherical symmetry. Using the conservation of the energy $E \equiv -g_{\mu\nu} k^\mu t^\nu$ and angular momentum $L \equiv g_{\mu\nu} k^\mu \phi^\nu$ and $k^\mu k_\mu = 0$, where k^μ is the photon wave number, the photon trajectory is given by

$$\frac{1}{r^4}\left(\frac{dr}{d\Phi}\right)^2 = \frac{1}{b^2} - \frac{1}{r^2}\left(1 - \frac{r_g}{r}\right), \tag{2.3}$$

where $b \equiv L/E$ is the impact parameter of the photon.

From the photon trajectory (2.3), we obtain

$$\frac{1}{2}\dot{r}^2 + V_{eff}(r) = 0, \tag{2.4}$$

where

$$V_{eff}(r) \equiv \frac{L^2}{2}\left[\frac{1}{r^2}\left(1 - \frac{r_g}{r}\right) - \frac{1}{b^2}\right] \tag{2.5}$$

and the dot represents the derivation with the affine parameter of the geodesic. The maximal value of the effective potential V_{eff} is

$$V_{eff}\left(\frac{3r_g}{2}\right) = \frac{L^2}{2}\left(\frac{4}{27r_g^2} - \frac{1}{b^2}\right). \tag{2.6}$$

Figure 2.2 shows that the photon is scattered if $b_c \equiv \frac{3\sqrt{3}r_g}{2} < |b|$, while reaches the horizon if $b_c > |b|$ because the photon trajectory is prohibited in the regions $V_{eff} < 0$. Since we are interested in the scattering problem, we assume $b_c < |b|$.

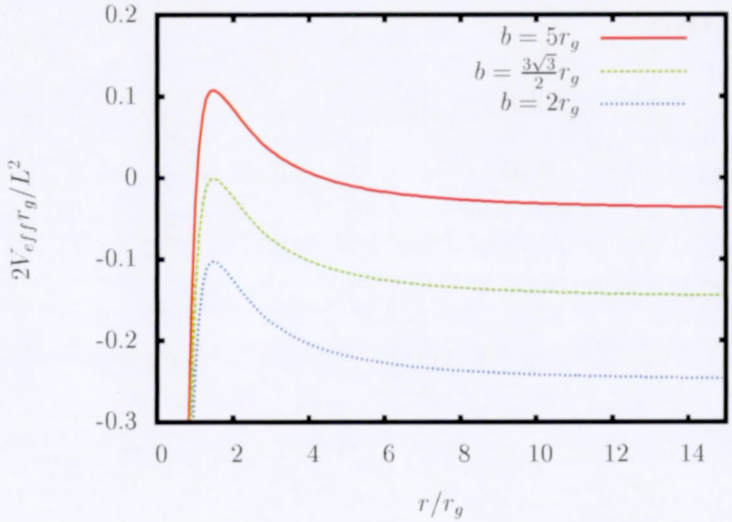

Figure 2.2: The effective potentials of the photon trajectories. The solid, broken and dot lines are the effective potentials with $b = 5r_g$, $b = \frac{3\sqrt{3}}{2}r_g$ and $b = 2r_g$, respectively. The photons which are emitted by sources with $\frac{3\sqrt{3}r_g}{2} < |b|$ reflect at $V_{eff} = 0$.

Using $u \equiv \frac{1}{r}$, $u_b \equiv \frac{1}{b}$, and $u_g \equiv \frac{1}{r_g}$, we get

$$\left(\frac{du}{d\Phi}\right)^2 = G(u), \tag{2.7}$$

where the function $G(u)$ is defined by

$$G(u) \equiv u_b^2 - u^2 + \frac{u^3}{u_g}. \tag{2.8}$$

In the scattering case, $G(u)$ has three zeros u_-, u_+ and u_0 which satisfy $u_- < 0 < u_+ < u_0 < u_g$. We can also describe $G(u)$ as

$$G(u) = \frac{1}{u_g}(u - u_-)(u - u_+)(u - u_0). \tag{2.9}$$

By comparing Eq. (2.8) with Eq. (2.9), we can find

$$\begin{aligned}
u_- &= \frac{r_+ - r_g - \sqrt{(r_+ - r_g)(r_+ + 3r_g)}}{2r_g r_+}, \\
u_+ &= \frac{1}{r_+}, \\
u_0 &= \frac{r_+ - r_g + \sqrt{(r_+ - r_g)(r_+ + 3r_g)}}{2r_g r_+},
\end{aligned} \tag{2.10}$$

where r_+ is the closest distance of the light ray. The relations

$$u_- + u_+ + u_0 = u_g \tag{2.11}$$

is very useful. The impact parameter b of the light ray is described by

$$b^2 = \frac{r_+^3}{r_+ - r_g}. \tag{2.12}$$

Figure 2.3 shows the deflection of the light ray. The light ray which comes from the direction $\Phi = -\alpha/2 - \pi/2$ is deflected at $\Phi = 0$ and goes away in the direction $\Phi = \alpha/2 + \pi/2$. The deflection angle α of the light ray is calculated as

$$\alpha = 2\int_0^{u_+} \frac{du}{\sqrt{G(u)}} - \pi. \tag{2.13}$$

This integral is expressed in terms of an incomplete elliptic integral of the first kind $F(\varphi, k)$ which is defined by

$$F(\varphi, k) = \int_0^{\varphi} \frac{d\vartheta}{\sqrt{1 - k^2 \sin^2 \vartheta}} \tag{2.14}$$

and the complete elliptic integral of the first kind $K(k)$ which is defined as $K(k) \equiv F(\pi/2, k)$ [54, 55]. (For example, see for the details of the elliptic integrals [56].) Thus, the deflection angle α of the light ray is given by

$$\begin{aligned}
\alpha &= 2\sqrt{u_g}\int_0^{u_+} \frac{du}{\sqrt{(u-u_-)(u-u_+)(u-u_0)}} - \pi \\
&= 2\sqrt{u_g}\left(\int_{u_-}^{u_+} \frac{du}{\sqrt{(u-u_-)(u-u_+)(u-u_0)}}\right. \\
&\qquad \left. - \int_{u_-}^{0} \frac{du}{\sqrt{(u-u_-)(u-u_+)(u-u_0)}}\right) - \pi \\
&= \frac{4\sqrt{u_g}}{\sqrt{u_0 - u_-}}\left[K(k_1) - F(\varphi_1, k_1)\right] - \pi,
\end{aligned} \tag{2.15}$$

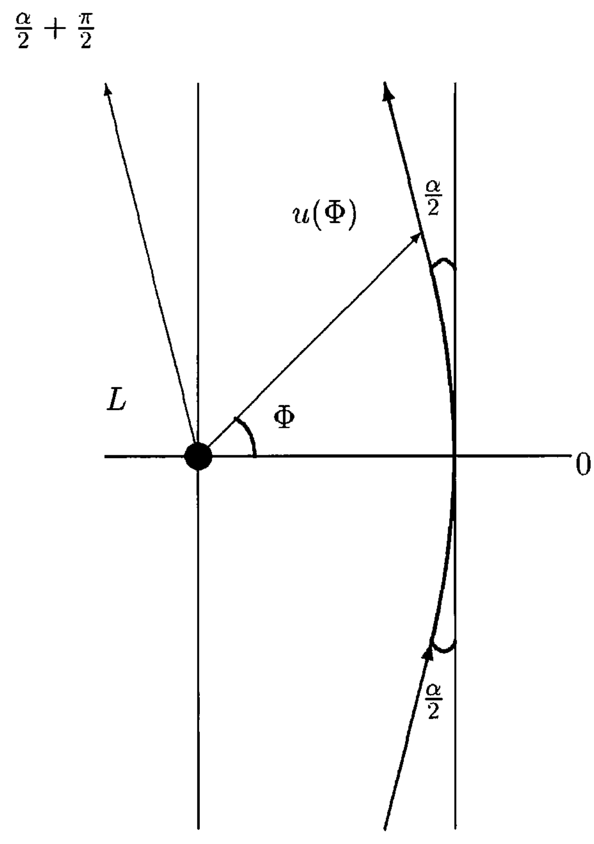

Figure 2.3: The deflection of the light ray. The light ray which comes from the direction $\Phi = -\alpha/2 - \pi/2$ is deflected at $\Phi = 0$ and goes away the direction $\Phi = \alpha/2 + \pi/2$.

where

$$k_1 \equiv \sqrt{\frac{u_+ - u_-}{u_0 - u_-}} = \sqrt{\frac{\sqrt{(r_+ - 2m)(r_+ + 6m)} - r_+ + 6m}{2\sqrt{(r_+ - 2m)(r_+ + 6m)}}} \tag{2.16}$$

and

$$\varphi_1 \equiv \arcsin\sqrt{\frac{-u_-}{u_+ - u_-}} = \arcsin\sqrt{\frac{\sqrt{(r_+ - 2m)(r_+ + 6m)} - r_+ + 2m}{\sqrt{(r_+ - 2m)(r_+ + 6m)} - r_+ + 6m}} \tag{2.17}$$

In the strong field limit $b \to b_c$, $u_+ \simeq u_0 \to 2u_g/3$ and $u_- \to -u_g/3$ and hence

$$k_1 \to 1, \tag{2.18}$$

$$\varphi_1 \to \arcsin\sqrt{\frac{1}{3}} \tag{2.19}$$

and

$$\sqrt{u_0 - u_-} \to \sqrt{u_g}. \tag{2.20}$$

Therefore, the deflection angle of the light ray in the strong field limit is given by

$$\begin{aligned} \alpha &\simeq 4\left[K(k_1) - F\left(\arcsin\sqrt{\frac{1}{3}}, k_1\right)\right] - \pi \\ &\to \log\infty. \end{aligned} \tag{2.21}$$

This implies that the light ray winds around the black hole nearly on the photon sphere in the strong field limit.

In the weak field approximation $b \gg r_g$, from Eq. (2.15), the deflection angle is given by [53, 55]

$$\alpha \simeq \frac{2r_g}{b}. \tag{2.22}$$

2.3 Schwarzschild lens in the weak field

In this section we review the Schwarzschild lens under the weak field approximation [3, 6]. This review in brief would help us to understand Sec. 4.1, Sec. 4.2 and Sec. 6.2.

In this case, the effective deflection angle is $\bar{\alpha} = \alpha$ or the winding number of light is $n = 0$. Using by the deflection angle (2.22) and $b = D_l\theta$, the lens equation (2.1) becomes

$$\hat{\theta}^2 - \hat{\phi}\hat{\theta} - 1 = 0, \tag{2.23}$$

where

$$\hat{\theta} \equiv \frac{\theta}{\theta_0}, \quad \hat{\phi} \equiv \frac{\phi}{\theta_0} \tag{2.24}$$

and

$$\theta_0 \equiv \sqrt{2\frac{D_{ls}}{D_s}\frac{r_g}{D_l}}. \tag{2.25}$$

When an observer has a linear view of a source and a lens object or $\phi = 0$, the ring image which is called Einstein ring with the image angle $2\theta_0$ is formed for the spherical symmetry. The solutions of the lens equation are

$$\hat{\theta}_\pm = \frac{1}{2}\left(\hat{\phi} \pm \sqrt{\hat{\phi}^2 + 4}\right). \tag{2.26}$$

So the separation of two images is given by

$$\hat{\theta}_+ - \hat{\theta}_- = \sqrt{\hat{\phi}^2 + 4}. \tag{2.27}$$

The solutions have some relations which given by

$$\begin{aligned} \hat{\theta}_+ + \hat{\theta}_- &= \hat{\phi}, & (2.28)\\ \hat{\theta}_+\hat{\theta}_- &= -1, & (2.29)\\ -\hat{\theta}_- < 1 &< \hat{\theta}_+. & (2.30) \end{aligned}$$

If the source object is far away from the lens object on the source plain $\hat{\phi} \gg 1$, the image angles are

$$\hat{\theta}_+ = \hat{\phi} + \frac{1}{\hat{\phi}}, \quad \hat{\theta}_- = -\frac{1}{\hat{\phi}}. \tag{2.31}$$

Then,

$$\frac{d\hat{\theta}_\pm}{d\hat{\phi}} = \frac{1}{2} \pm \frac{1}{2}\hat{\phi}(\hat{\phi}^2 + 4)^{-\frac{1}{2}} \tag{2.32}$$

and the signed magnifications are

$$\mu_{0\pm} \equiv \frac{\hat{\theta}_\pm}{\hat{\phi}} \frac{d\hat{\theta}_\pm}{d\hat{\phi}} = \frac{1}{2} \pm \frac{1}{4} \left(\frac{\hat{\phi}}{\sqrt{\hat{\phi}^2 + 4}} + \frac{\sqrt{\hat{\phi}^2 + 4}}{\hat{\phi}} \right). \tag{2.33}$$

The signed magnification sum $\mu_{0+} + \mu_{0-}$ is always unity. The absolute values of the magnifications are given by

$$|\mu_{0\pm}| = \frac{1}{4} \left(\frac{\hat{\phi}}{\sqrt{\hat{\phi}^2 + 4}} + \frac{\sqrt{\hat{\phi}^2 + 4}}{\hat{\phi}} \right) \pm \frac{1}{2}. \tag{2.34}$$

The total magnification is obtained by

$$\mu_0 \equiv |\mu_{0+}| + |\mu_{0-}| = \frac{\hat{\phi}^2 + 2}{\hat{\phi}\sqrt{\hat{\phi}^2 + 4}} \geqq 1. \tag{2.35}$$

Thus, the total image always is magnified. The ratio of the magnification is

$$\frac{|\mu_{0+}|}{|\mu_{0-}|} = \left(\frac{\sqrt{4 + \hat{\phi}^2} + \hat{\phi}}{\sqrt{4 + \hat{\phi}^2} - \hat{\phi}} \right)^2. \tag{2.36}$$

Chapter 3

Ellis spacetime

The Ellis spacetime was investigated as a geodesically complete particle model by Ellis [57] and turned out to describe a wormhole connecting two Minkowski spacetimes. The Ellis spacetime is a static, spherically symmetric, asymptotically flat solution of the Einstein equation with a massless scalar field with a wrong sign as a matter field. It is well known that such a matter field violates energy conditions and it could represent the negative energy density from quantum effects, such as the Casimir effect. This spacetime is the simplest and earliest example of wormholes proposed by Morris and Thorne [58, 59]. This is a traversable wormhole in the sense that an observer can cross this wormhole in both directions.

In this chapter, we briefly review Morris-Thorne wormhole [58], the Ellis spacetime [57] and the deflection angle in the Ellis spacetime [52, 60, 61].

3.1 Morris-Thorne wormhole

In this section, we will briefly review the Morris-Thorne wormhole [58]. The line element of the static and spherically spacetime can be described by

$$ds^2 = -e^{2A(r)}dt^2 + \frac{dr^2}{1-\frac{B(r)}{r}} + r^2 d\Theta^2 + r^2 \sin^2\Theta d\Phi^2, \tag{3.1}$$

where $B(r)$ and $A(r)$ are arbitrary functions of r. If we set $A(r) = 0$ and $B(r) = a^2/r$, where a is a positive constant, the spacetime is the Ellis wormhole spacetime. We use a set of orthonormal basis vectors

$$\boldsymbol{e}_{\hat{t}} = e^{-A}\boldsymbol{e}_t, \tag{3.2}$$

$$\boldsymbol{e}_{\hat{r}} = \sqrt{1-\frac{B}{r}}\boldsymbol{e}_r, \tag{3.3}$$

$$e_{\hat{\Theta}} = \frac{1}{r} e_{\Theta}, \tag{3.4}$$
$$e_{\hat{\Phi}} = \frac{1}{r\sin\Theta} e_{\Phi}. \tag{3.5}$$

The non-zero components of the Einstein tensor $G_{\hat{\mu}\hat{\nu}}$ are

$$G_{\hat{t}\hat{t}} = \frac{B'}{r^2}, \tag{3.6}$$
$$G_{\hat{r}\hat{r}} = -\frac{B}{r^3} + 2\left(1 - \frac{B}{r}\right)\frac{A'}{r}, \tag{3.7}$$
$$G_{\hat{\Theta}\hat{\Theta}} = G_{\hat{\Phi}\hat{\Phi}} = \left(1 - \frac{B}{r}\right)\left(A'' - \frac{B'r - B}{2r(r-B)}A' + (A')^2 + \frac{A'}{r} - \frac{B'r - B}{2r^2(r-B)}\right). \tag{3.8}$$

From the symmetry, the non-zero components of the stress-energy tensor $T_{\hat{\mu}\hat{\nu}}$ are

$$T_{\hat{t}\hat{t}} = \rho(r), \quad T_{\hat{r}\hat{r}} = -\tau(r), \quad T_{\hat{\Theta}\hat{\Theta}} = T_{\hat{\Phi}\hat{\Phi}} = p(r), \tag{3.9}$$

where $\rho(r)$ is the total density of mass-energy that static observers measure, $\tau(r)$ is the tension per unit area that they measure in the radial direction and $p(r)$ is the pressure that they measure in the directions orthogonal to radial.

From the Einstein equations

$$G_{\hat{\mu}\hat{\nu}} = 8\pi T_{\hat{\mu}\hat{\nu}}, \tag{3.10}$$

the Einstein tensor (3.6)-(3.8) and the stress-energy tensor (3.9), we obtain the equations

$$B' = 8\pi G r^2 \rho, \tag{3.11}$$
$$A' = \frac{-8\pi G\tau r^3 + B}{2r(r-B)}, \tag{3.12}$$
$$\tau' = (\rho - \tau)A' - 2\frac{p+\tau}{r}, \tag{3.13}$$

or

$$\rho = \frac{B'}{8\pi G r^2}, \tag{3.14}$$
$$\tau = \frac{B - 2(r-B)rA'}{8\pi G r^3}, \tag{3.15}$$
$$p = \frac{r}{2}[(\rho - \tau)A' - \tau'] - \tau. \tag{3.16}$$

We define a dimensionless function ζ as

$$\zeta \equiv \frac{\tau - \rho}{|\rho|} = \frac{B - rB' - 2(r - B)rA'}{r\,|B'|}. \tag{3.17}$$

Embedding diagram is a useful tool to understand wormhole spacetimes. We embed the two dimensional surface with the line element

$$ds^2 = \frac{dr^2}{1 - \frac{B(r)}{r}} + r^2 d\Phi^2, \tag{3.18}$$

which is the line element (3.1) by setting $t = constant$ and $\Theta = \frac{\pi}{2}$ in the Euclidean space. We introduce cylindrical coordinates z, r and Φ and the line element of the embedding space is described by

$$ds^2 = dz^2 + dr^2 + r^2 d\Phi^2. \tag{3.19}$$

The line element of the embedded two-dimensional surface can be described

$$ds^2 = \left[1 + \left(\frac{dz}{dr}\right)^2\right] dr^2 + r^2 d\Phi^2, \tag{3.20}$$

where $z = z(r)$ is an embedding function. If we identify the coordinates r and Φ of Eq. (3.18) with the ones of Eq. (3.20), the embedding function z should satisfy

$$\frac{dz}{dr} = \pm\sqrt{\frac{1}{\frac{r}{B} - 1}} = \pm\sqrt{\frac{B}{r - B}}. \tag{3.21}$$

Wormholes must have a minimum radius $r = B_0$ which is called the throat of the wormhole. Since the embedded surface is vertical at the throat, from Eq. (3.21), $B = r$. Thus, $r = B = B_0$ at the throat. The inverse of the embedding function $r(z)$ have to satisfy

$$\frac{d^2r}{dz^2} = \frac{B - rB'}{2B^2} > 0. \tag{3.22}$$

at or near the throat $r = B = B_0$ to connect two asymptotically flat regions. From Eqs. (3.17) and (3.22), the dimensionless function ζ is given by

$$\zeta = \frac{2B^2}{r\,|B'|}\left(\frac{d^2r}{dz^2}\right) - \frac{2(r - B)A'}{|B'|}. \tag{3.23}$$

We assume the energy density ρ is finite. From Eq. (3.11), B' should be finite and hence $(r - B)A'$ must vanish at the throat. Therefore, the dimensionless function $\zeta_0 \equiv \zeta(r = B = B_0)$ is positive at the throat. From the definition of the dimensionless function ζ, (See Eq. (3.17),) we realize that wormholes need to be composed of an exotic matter with $\tau_0 \equiv \tau(r = B = B_0) > \rho_0 \equiv \rho(r = B = B_0)$. This implies that we need exotic matters near the wormhole throat at least which violate the null energy condition $T_{\mu\nu}k^\mu k^\nu \geq 0$, where k^μ is an arbitrary, future-directed null vector.

However, if we consider gravitational theories with an adding term $H_{\mu\nu}$ and the modified Einstein equations which are described by

$$G_{\mu\nu} + H_{\mu\nu} = T_{\mu\nu}, \tag{3.24}$$

the analysis for the Morris-Thorne wormhole only implies that the condition $(T_{\mu\nu} - H_{\mu\nu})\, k^\mu k^\nu \geq 0$ is violated near the throat. Thus, we does not always need exotic matters violating the null energy condition for wormholes in this case.

Formation of wormholes

Various wormhole solutions have been found still now but the formation of wormholes is still a open question. Recently, a simple analytic model of wormhole formation from the initial data with a massless ghost scalar field has been investigated by Maeda [70]. It may be important to note that a curvature singularity appears when the wormhole is formed. Cosmological wormholes which are formed from initial singularities also have been investigated [71, 72, 73, 74].

3.2 Ellis spacetime in brief

In this section, we review the Ellis spacetime which is the simplest and earliest solution of the Morris-Thorne class [57]. The line element of the static and spherically symmetric spacetime is described by

$$\begin{aligned} ds^2 &= -dt^2 + [d\rho - f(\rho)dt]^2 + r^2(\rho)(d\Theta^2 + \sin^2\Theta d\Phi^2) \\ &= -(1 - f(\rho)^2)dt^2 + d\rho^2 - 2f(\rho)dtd\rho + r^2(\rho)\left(d\Theta^2 + \sin^2\Theta d\Phi^2\right), \end{aligned} \tag{3.25}$$

where $r(\rho)$ is non-negative and the range of the coordinate is given by $-\infty < t < \infty$, $-\infty < \rho < \infty$, $0 < \Theta < \pi$ and $-\pi < \Phi < \pi$. The determinant g of the metric tensor $g_{\mu\nu}$ is obtained by

$$g = -r^4 \sin^2\Theta. \tag{3.26}$$

Ellis introduced the vector field $\boldsymbol{u}$ which is orthogonal to the hypersurface $t =$ constant

$$u^\mu \partial_\mu = -\partial_t - f(\rho)\partial_\rho. \tag{3.27}$$

We use an orthonormal frame system $\{\boldsymbol{e}_\mu\}$

$$\boldsymbol{e}_0 = \boldsymbol{u} = -\partial_t - f(\rho)\partial_\rho, \tag{3.28}$$

$$\boldsymbol{e}_1 = \partial_\rho, \tag{3.29}$$

$$\boldsymbol{e}_2 = \frac{1}{r(\rho)}\partial_\Theta, \tag{3.30}$$

$$\boldsymbol{e}_3 = \frac{1}{r(\rho)\sin\Theta}\partial_\Phi. \tag{3.31}$$

The non-zero components of the Ricci curvature tensor $R_{\mu\nu}$ are obtained by

$$R_{00} = -\frac{(r^2 f f')'}{r^2} - \frac{2r'' f^2}{r}, \tag{3.32}$$

$$R_{01} = \frac{2r'' f}{r}, \tag{3.33}$$

$$R_{11} = \frac{(r^2 f f')'}{r^2} - \frac{2r''}{r}, \tag{3.34}$$

$$R_{22} = R_{33} = \frac{1 - \left[r r' \left(1 - f^2\right)\right]'}{r^2}. \tag{3.35}$$

We consider the Lagrangian described by

$$L = R^\mu{}_\mu + K\chi^{;\mu}\chi_{;\mu}, \tag{3.36}$$

where K is the non-zero coupling constant and χ is a scalar field which is described by

$$\chi = \gamma(\rho), \tag{3.37}$$

where $\gamma(\rho)$ is a non-constant, differentiable, real-valued function. From the variational principle, we obtain

$$0 = \delta \int \sqrt{-g}\left(R^\mu{}_\mu + K\chi^{;\mu}\chi_{;\mu}\right) d^4x. \tag{3.38}$$

If $K > 0$, then r is convex while if $K < 0$, then r is concave [57]. We take $K > 0$ to remove the Schwarzschild singularity and to make a throat and we will set $K = 2$ with rescaling χ. From Eq. (3.38), we get the Einstein equations

$$R_{\mu\nu} - \frac{1}{2}R^\lambda{}_\lambda g_{\mu\nu} = -2\left(\chi_{;\mu}\chi_{;\nu} - \frac{1}{2}\chi^{;\lambda}\chi_{;\lambda}g_{\mu\nu}\right) \tag{3.39}$$

and the scalar wave equation

$$\chi^{;\mu}{}_{;\mu} = 0. \tag{3.40}$$

The Einstein equations (3.39) are also expressed by

$$R_{\mu\nu} = -2\chi_{;\mu}\chi_{;\nu}. \tag{3.41}$$

The wave equation (3.40) yields

$$\left[r^2\left(f^2-1\right)\gamma'\right]' = 0. \tag{3.42}$$

The $(0-0)$, $(0-1)$, $(1-1)$ and $(2-2)$ components of the Einstein equations (3.41) are obtained by

$$\frac{(r^2 ff')'}{r^2} + \frac{2r''f^2}{r} = 2f^2\gamma'^2, \tag{3.43}$$

$$\frac{2r''f}{r} = 2f\gamma'^2, \tag{3.44}$$

$$-\frac{(r^2 ff')'}{r^2} + \frac{2r''}{r} = 2\gamma'^2 \tag{3.45}$$

and

$$\frac{\left[rr'\left(1-f^2\right)\right]' - 1}{r^2} = 0, \tag{3.46}$$

respectively. The $(3-3)$ component is equal to the $(2-2)$ component for the spherical symmetry. Equations (3.43)-(3.46) are equivalent to the three equations

$$\frac{r''}{r} = \gamma'^2, \tag{3.47}$$

$$\left(r^2 ff'\right)' = 0, \tag{3.48}$$

$$\left[rr'(1-f^2)\right]' = 1. \tag{3.49}$$

We can integrate Eqs. (3.48) and (3.49) and we get

$$r^2(1-f^2)' = 2m, \tag{3.50}$$

$$\left(r^2\right)'(1-f^2) = 2(\rho - m), \tag{3.51}$$

where m is an integration constant and the zero point of ρ has been adjusted to equalize two integration constants. From Eqs. (3.50) and (3.51), it follows that

$$r^2(1-f^2) = \rho^2 + C, \tag{3.52}$$

where C is an integration constant. From Eqs. (3.42) and (3.52), we obtain

$$\gamma' = \frac{-l}{r^2(1-f^2)} = \frac{-l}{\rho^2+C}, \tag{3.53}$$

where l is an integration constant. From Eqs. (3.51) and (3.52), we get

$$\frac{r'}{r} = \frac{\rho - m}{\rho^2 + C} \tag{3.54}$$

and

$$\frac{r''}{r} = \frac{C+m^2}{(\rho^2+C)^2}. \tag{3.55}$$

From Eqs. (3.47), (3.53) and (3.55), it follows that

$$C = l^2 - m^2. \tag{3.56}$$

Equations (3.53), (3.54) and (3.56) imply that

$$r^2(\rho) = \left|\rho^2 + l^2 - m^2\right| \exp\left[\frac{2m\gamma(\rho)}{l}\right]. \tag{3.57}$$

Here we introduce a new coordinate T satisfying

$$dT = dt + \frac{f(\rho)}{1-f^2(\rho)} d\rho. \tag{3.58}$$

The line element (3.25) is described by

$$ds^2 = -\left[1 - f^2(\rho)\right] dT^2 + \frac{d\rho^2}{1-f^2(\rho)} + r^2(\rho)\left(d\Theta^2 + \sin^2\Theta d\Phi^2\right). \tag{3.59}$$

From Eqs. (3.52), (3.56) and (3.57), the line element (3.59) is expressed by

$$ds^2 = \mathrm{sgn}(\rho^2 + l^2 - m^2)\left\{-e^{-\frac{2m\gamma(\rho)}{l}} dT^2 + e^{\frac{2m\gamma(\rho)}{l}}\left[d\rho^2 + \left(\rho^2 + l^2 - m^2\right) d\Omega^2\right]\right\}, \tag{3.60}$$

where $\mathrm{sgn}(x)$ is a sign function defined by

$$\mathrm{sgn}(x) \equiv \frac{x}{|x|}. \tag{3.61}$$

In the following, we will make an analysis for case where $l^2 > m^2$. (See Ellis [57] for the cases where $l^2 < m^2$ and $l^2 = m^2$.) To simplify the discussion, we assume that the integration constants m and l are non-negative. From Eqs. (3.52), (3.53), (3.56) and (3.57), it follows that

$$\gamma'(\rho) = -\frac{l}{\rho^2 + a^2}, \tag{3.62}$$

$$r^2(\rho) = (\rho^2 + a^2)e^{\frac{2m\gamma(\rho)}{l}}, \tag{3.63}$$

$$f^2(\rho) = 1 - e^{-\frac{2m\gamma(\rho)}{l}}, \tag{3.64}$$

and hence

$$\gamma(\rho) = \frac{l}{a}\left[\frac{\pi}{2} - \arctan\frac{\rho}{a}\right], \tag{3.65}$$

where $a \equiv \sqrt{l^2 - m^2}$ and we have applied the boundary condition

$$\lim_{\rho\to\infty} \chi = \lim_{\rho\to\infty} \gamma(\rho) = 0. \tag{3.66}$$

Under this boundary condition, γ is everywhere positive.

The derivatives of $f^2(\rho)$ and $r^2(\rho)$ are given by

$$\frac{d(f^2)}{d\rho} = -\frac{2m}{\rho^2 + a^2}e^{-\frac{2m\gamma}{l}} \tag{3.67}$$

and

$$\frac{d(r^2)}{d\rho} = e^{\frac{2m\gamma}{l}}(2\rho - 2m), \tag{3.68}$$

respectively. Under the assumption $m \geq 0$ and $l \geq 0$, $f^2(\rho)$ is monotonically decreasing with respect to the coordinate ρ and changes from $1 - e^{\frac{2m\pi}{a}}$ to 0 as ρ increases from $-\infty$ to ∞ and r^2 has a minimal value at $\rho = m$.

The asymptotic behavior is given by

$$r(\rho) = \rho + m + O\left(\frac{1}{\rho}\right), \tag{3.69}$$

$$f^2(\rho) = \frac{2m}{\rho + m} + O\left(\frac{1}{\rho^2}\right) \tag{3.70}$$

as $\rho \to \infty$ and

$$r(\rho) = -e^{\frac{m\pi}{a}}(\rho + m) + O\left(\frac{1}{\rho}\right), \tag{3.71}$$

$$f^2(\rho) = 1 - e^{-\frac{2m\pi}{a}}\left(1 - \frac{2m}{\rho + m}\right) + O\left(\frac{1}{\rho^2}\right) \tag{3.72}$$

as $\rho \to -\infty$. Equations (3.69) and (3.70) and the line element (3.59) imply that the Ellis spacetime is asymptotic to Schwarzschild spacetime with the mass parameter m as $\rho \to \infty$. As $\rho \to -\infty$, from Eqs. (3.71) and (3.72), the line element (3.59) is asymptotic to

$$ds^2 = -\left(1 + \frac{2me^{\frac{m\pi}{a}}}{r}\right) d\left(e^{-\frac{m\pi}{a}}T\right)^2 + \frac{dr^2}{1 + \frac{2me^{\frac{m\pi}{a}}}{r}} + r^2\left(d\Theta^2 + \sin^2\Theta d\Phi^2\right). \quad (3.73)$$

This implies that the Ellis spacetime is asymptotic to Schwarzschild spacetime with the mass parameter $-me^{\frac{m\pi}{a}}$ as $\rho \to -\infty$.

The case $m = 0$, $f(\rho)$ vanishes from Eq. (3.64). From Eq. (3.63), it follows that

$$r^2(\rho) = \rho^2 + a^2 = \rho^2 + l^2 \quad (3.74)$$

and the line element (3.59) is obtained by

$$d\tau^2 = -dT + d\rho^2 + (\rho^2 + a^2)\left(d\Theta^2 + \sin^2\Theta d\Phi^2\right). \quad (3.75)$$

In this thesis, we will concentrate on the case $m = 0$ and we will name the Ellis spacetime with $m = 0$ the Ellis wormhole spacetime tentatively.

Introducing $R^2 = \rho^2 + a^2$, we can rewrite this into

$$ds^2 = -dT^2 + \left(1 - \frac{a^2}{R^2}\right)^{-1} dR^2 + R^2 d\Omega^2, \quad (3.76)$$

where $R = \pm a$ corresponds to the wormhole throat.

Upper bound of the number density

It seems that wormholes cannot be bright unlike stars. Thus, gravitational lensing is a useful tool to search wormholes. The Sloan Digital Sky Survey Quasar Lens Search [62, 63, 64, 65] has the largest quasar lens sample in the Sloan Digital Sky Survey [66]. There are 50,836 quasars with the redshift $z = 0.6 - 2.2$ and the apparent magnitude brighter than $i = 19.1$ and 19 lensed quasars are found. However, there is no lensed image by the unseen lens objects including the Ellis wormhole. Recently, Takahashi and Asada [51] presented the upper bound of the number density $\leq 10^{-4}h^3\mathrm{Mpc}^{-3}$ of the Ellis wormholes for a range of the throat radius $10^1 \leq a \leq 10^4\mathrm{pc}$ by using the Sloan Digital Sky Survey Quasar Lens Search.

The femto-lensing by the gamma-ray bursts can constrain the abundance of compact objects [67]. Yoo *et al.* [68] gave the upper bound of the number density $\leq 10^{-9}\mathrm{AU}^{-3}$ of the Ellis wormholes with the throat $\simeq 1\mathrm{cm}$ by data of the Fermi Gamma-ray Burst Monitor [69].

Instability

The Ellis wormhole is unstable with respect to unrestricted linear perturbations of the metric and the scalar field [75] and Armendáriz-Picón showed that the Ellis wormhole is stable with a restricted perturbation which is required to vanish at the throat [76]. Nonlinear instabilities of the Ellis wormhole were also investigated [77, 78, 79]. Needless to say, it does not imply that stable wormholes do not exit. The stability of a phantom static wormhole with thin shells for the linearized spherically symmetric perturbation was found by Lobo [80]. Static wormholes are too simple and realistic wormholes with the cosmological evolution should be described in dynamical situations [71, 72, 73, 74, 81, 82, 83, 84]. Although the Ellis wormhole is unstable, we will research the gravitational lensing effect by the Ellis wormhole because of the simplicity of the gravitational lensing configuration in this thesis.

Other matters

Ellis wormhole geometry is obtained with a Kalb-Ramond axion [85] and with tachyon matter and a positive cosmological constant [86] as a source.

Gravitational lensing

Chetouani and Clement derived the deflection angle of light in the Ellis wormhole spacetime and calculated the scattering cross-section [60]. Perlick investigated the gravitational lensing effects of the light ray through the Ellis wormhole throat by using the full lens equation [33] and Nandi *et al.* [14] applied the analysis of the strong field limit [28, 29, 30, 31].

It was pointed out that the qualitative features of gravitational lensing in the Ellis wormhole spacetime are similar to the ones in the Schwarzschild spacetime [14, 33, 87]. However, Abe showed that one can distinguish between the Ellis wormholes and mass lens objects with their light curves in the weak field limit [88] (see Appendix B). The Ellis wormholes could be detected with the astrometric image centroid trajectory in the weak field limit [89].

Recently, Nakajima and Asada [61] recalculated the deflection angle of light on the Ellis wormhole spacetime and proved that Dey and Sen [16]'s calculation is only correct at the lowest order in the weak field limit, while the conclusions by Abe [88] and Toki *et al.* [89] are still valid.

3.3 Deflection angle in the Ellis wormhole spacetime

In this section, we review the deflection angle on the Ellis wormhole spacetime [60, 61].

We can concentrate ourselves on the equatorial plane because of spherical symmetry. The photon trajectory with the metric (3.76) is given by

$$\frac{1}{R^4}\left(\frac{dR}{d\Phi}\right)^2 = \frac{1}{b^2}\left(1-\frac{a^2}{R^2}\right)\left(1-\frac{b^2}{R^2}\right), \tag{3.77}$$

where b is the impact parameter of the photon.

We can see that the photon is scattered if $|b| > a$, while reaches the throat if $|b| < a$. Since we are interested in the scattering problem, we assume $|b| > a$. Using $u \equiv 1/R$, we find

$$\left(\frac{du}{d\Phi}\right)^2 = \frac{1}{b^2}(1-a^2u^2)(1-b^2u^2). \tag{3.78}$$

Putting

$$G(u) = a^2(a^{-2}-u^2)(b^{-2}-u^2), \tag{3.79}$$

the azimuthal angle Φ can be given as a function of u by

$$\Phi = \pm\int_u^{b^{-1}} \frac{du}{\sqrt{G(u)}}. \tag{3.80}$$

Here we have set $\Phi(b^{-1}) = 0$. The deflection angle α is then calculated to give

$$\alpha = 2\int_0^{b^{-1}} \frac{du}{\sqrt{G(u)}} - \pi. \tag{3.81}$$

In the present case, we find

$$\int_0^{b^{-1}} \frac{du}{\sqrt{G(u)}} = \int_0^{\pi/2} \frac{d\vartheta}{\sqrt{1-\left(\frac{a}{b}\right)^2\sin^2\vartheta}} = K\left(\frac{a}{b}\right), \tag{3.82}$$

where we have transformed $u = b^{-1}\sin\vartheta$. Since $K(k)$ admits a power series

$$K(k) = \frac{\pi}{2}\sum_{n=0}^{\infty}\left[\frac{(2n-1)!!}{(2n)!!}\right]^2 k^{2n}, \tag{3.83}$$

where $n!!$ denotes the double factorial of n and $(-1)!! = 1$. The deflection angle is given by

$$\alpha = 2K\left(\frac{a}{b}\right) - \pi. \tag{3.84}$$

We get the deflection angle

$$\alpha = \pi \sum_{n=1}^{\infty} \left[\frac{(2n-1)!!}{(2n)!!}\right]^2 \left(\frac{a}{b}\right)^{2n}. \tag{3.85}$$

Thus, the deflection angle is approximately given in the weak-field regime $|b| \gg a$ by

$$\alpha \simeq \frac{\pi}{4}\left(\frac{a}{b}\right)^2. \tag{3.86}$$

In general, the deflection angle is always greater than its weak-field approximation and is diverging as $|b| \to a$.

Chapter 4

Gravitational lenses in the weak field

It is well known that the sum of signed magnifications is invariant in the weak field limit for mass lens systems. If gravitational lenses of the exotic lens object break the magnification invariance, the sum of signed magnifications would be a powerful tool to detect exotic lens objects.

In this chapter, we will discuss the signed magnification sums of general spherical lens models, including the singular isothermal sphere, the Schwarzschild lens and the Ellis wormhole in the weak field approximation [90].

4.1 The general spherical lens in the weak field

It is well known that the sum of signed magnifications is invariant for mass lens systems in the maximal-image domains. In this section, we will calculate the signed magnification sum of the general spherical lens model and we will number the real solutions of the lens equation because the signed magnification sums are physical invariants only when all the solutions are real [90].

We consider the general spherical lens model with the deflection angle, parametrized by

$$\alpha = \pm C b^{-n} = \pm \frac{C}{D_l^n} \theta^{-n}, \tag{4.1}$$

where C is a positive constant, n is a non-negative integer, b is the impact parameter of light rays emitted by a source and θ is the image angle and we have used the relation $b = D_l\theta$. If n is odd, then the sign is only the upper one, while if n is even, then the sign is the upper one for $\theta > 0$ and the lower one for $\theta < 0$. Thus, we have to treat two lens equations when n is even. This lens model describes the singular isothermal sphere, the Schwarzschild lens and the Ellis wormhole for $n = 0$, 1 and 2, respectively. The case where $n \geq 3$ would describe some exotic lens objects and the gravitational lens effect of modified gravitational theories. The following discussion in this chapter does not depend on the value of C.

The lens equation is given by

$$\hat{\theta}^{n+1} - \hat{\phi}\hat{\theta}^{n} \mp 1 = 0, \tag{4.2}$$

where

$$\hat{\theta} \equiv \frac{\theta}{\theta_0} \quad \text{and} \quad \hat{\phi} \equiv \frac{\phi}{\theta_0}, \tag{4.3}$$

and

$$\theta_0 \equiv \left(\frac{D_{ls}C}{D_s D_l^n}\right)^{\frac{1}{n+1}} \tag{4.4}$$

is the Einstein ring angle. We can concentrate ourselves on the case where the source angle ϕ is positive for symmetry. The solutions $\hat{\theta}_1$, $\hat{\theta}_2$, $\cdots$, $\hat{\theta}_{n+1}$ of the lens equation (4.2) of $(n+1)$-th degree satisfy

$$\prod_{i=1}^{n+1}(\hat{\theta} - \hat{\theta}_i) = 0. \tag{4.5}$$

For $n \geq 1$ we compare Eq. (4.2) with Eq. (4.5) and obtain

$$\sum_{i=1}^{n+1}\hat{\theta}_i = \hat{\phi}, \tag{4.6}$$

and

$$\sum_{i<j}\hat{\theta}_i\hat{\theta}_j = -\delta_{1n}, \tag{4.7}$$

where $\delta_{1n} = 0$ for $n \geq 2$ and $\delta_{1n} = 1$ for $n = 1$. Using the both equations, we obtain

$$\hat{\phi}^2 = \left(\sum_{i=1}^{n+1}\hat{\theta}_i\right)^2 = \sum_{i=1}^{n+1}\hat{\theta}_i^2 - 2\delta_{1n}. \tag{4.8}$$

This implies

$$\sum_{i=1}^{n+1} \frac{\hat{\theta}_i}{\hat{\phi}} \frac{d\hat{\theta}_i}{d\hat{\phi}} = 1. \tag{4.9}$$

Note that these solutions $\hat{\theta}_i$ may be complex and not all the magnifications are always physical and that Eq. (4.9) is satisfied regardless of the sign of Eq. (4.2).

Now we will count the number of the images. We can express the lens equation (4.2) as follows

$$\pm\hat{\theta}^{-n} = \hat{\theta} - \hat{\phi}. \tag{4.10}$$

In the following, we will make analysis for cases (i) where n is odd, (ii) where n is even and positive and (iii) where $n = 0$, separately.

(i) n is odd.

In the case where n is odd, the lens equation is given by

$$\hat{\theta}^{-n} = \hat{\theta} - \hat{\phi}. \tag{4.11}$$

The solutions are given by the intersections of $y = 1/x^n$ and $y = x - \hat{\phi}$. Figure 4.1 shows the left-hand side and the right-hand side of the lens equation and the intersections for $n = 1$.

We find a positive solution θ_+ and a negative solution θ_- regardless of the value for $\hat{\phi}$. We also can see the positive solution $\hat{\theta}_+ \simeq \hat{\phi}$ and the negative solution $\hat{\theta}_- \simeq 0$ for $\hat{\phi} \gg 1$. We also can see that $n = 1$ is the only case where all the solutions of the lens equation are real and the physical signed magnification sum is always unity. The lens with $n = 1$ and $C = 2r_g$ is the Schwarzschild lens. Thus, its signed magnification sum is always unity.

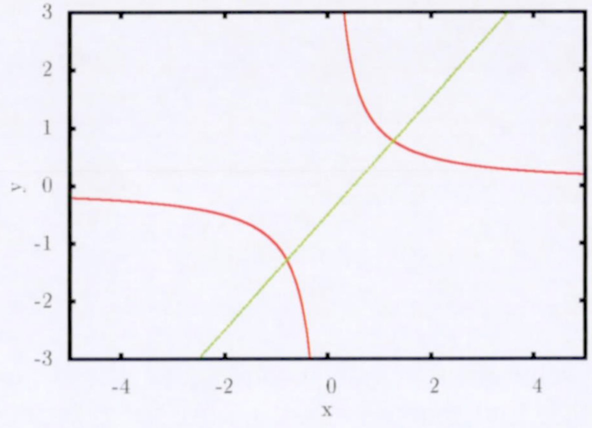

Figure 4.1: The solid (red) lines $y = 1/x^n$ and the broken (green) line $y = x-\hat{\phi}$, respectively, correspond to the left-hand side and the right-hand side of the lens equation (4.11) for $n = 1$ and $\hat{\phi} = 0.5$. The intersections correspond to the real solutions of the lens equation. This figure is taken from [90].

(ii) $n(\geq 2)$ **is even.**

We consider the case where $n \geq 2$ and is even. The lens equation is obtained by

$$\pm\hat{\theta}^{-n} = \hat{\theta} - \hat{\phi}. \tag{4.12}$$

The solutions are given by intersections of $y = 1/x^n$ for $x > 0$ and $y = -1/x^n$ for $x < 0$ and $y = x - \hat{\phi}$. This gives a figure which is very similar to Fig. 4.1 and we obtain a positive solution θ_+ and a negative solution θ_- regardless of the value for $\hat{\phi}$. The signed magnification sum (4.9) is not a physical quantity because it includes one or more non-real solutions in this case. The lens with $n = 2$ and $C = \pi a^2/4$ is the Ellis wormhole.

(iii) $n = 0$**.**

For $n = 0$, the lens equation is given by

$$\pm 1 = \hat{\theta} - \hat{\phi}. \tag{4.13}$$

The solutions are given by one or two intersections of $y = 1$ for $x > 0$ and $y = -1$ for $x < 0$ and $y = x - \hat{\phi}$. Figure 4.2 shows the left-hand side and the right-hand side of the lens equations and the intersections.

We obtain only one positive solution θ_+ in the range $\hat{\phi} > 1$ while we get a positive solution θ_+ and a negative solution θ_- in the range $0 \leq \hat{\phi} \leq 1$.
In the range $\hat{\phi} > 1$, by a straight forward calculation, we get

$$\frac{\hat{\theta}_+}{\hat{\phi}} \frac{d\hat{\theta}_+}{d\hat{\phi}} = 1 + \frac{1}{\hat{\phi}}. \tag{4.14}$$

In the range $0 \leq \hat{\phi} \leq 1$, we obtain

$$\frac{\hat{\theta}_\pm}{\hat{\phi}} \frac{d\hat{\theta}_\pm}{d\hat{\phi}} = 1 \pm \frac{1}{\hat{\phi}}. \tag{4.15}$$

Therefore the signed magnification sum is 2 in this range.
Only in the case $n = 0$, the number of images is not always 2. The singular isothermal sphere lens is given by setting $n = 0$ and $C = 4\pi\sigma^2$, where σ is the velocity dispersion of particles.

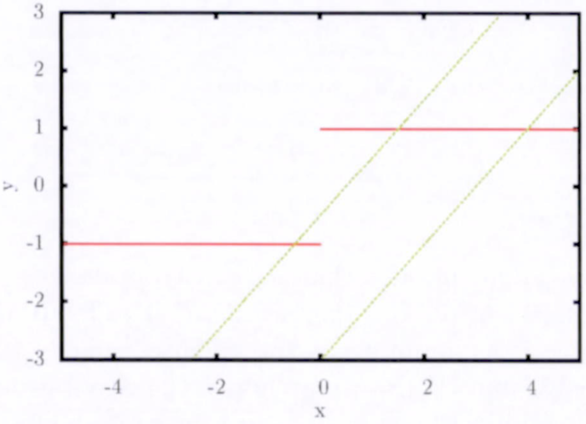

Figure 4.2: The solid (red) lines $y = 1$ for $x > 0$ and $y = -1$ for $x < 0$ and the broken (green) lines $y = x - \hat{\phi}$, respectively, correspond to the left-hand side and the right-hand side of the lens equation (4.13). We plot the lines in the case $\hat{\phi} = 0.5$ and $\hat{\phi} = 3$. The one or two intersections correspond to the real solutions of the lens equations. This figure is taken from [90].

For $\hat{\phi} > 0$, the positive solution $\hat{\theta}_+(\hat{\phi})$ and the negative solution $\hat{\theta}_-(\hat{\phi})$ of the lens equation (4.2) represent an outer image angle and an inner image angle while $\hat{\theta}_+(\hat{\phi})$ and $\hat{\theta}_-(\hat{\phi})$ are an inner one and an outer one for $\hat{\phi} < 0$, respectively. The positive solution $\hat{\theta}_+$ monotonically increases as $\hat{\phi}$ increases.

The signed magnifications of the images in the weak field limit are given by

$$\mu_{0\pm}(\hat{\phi}) \equiv \frac{\hat{\theta}_\pm(\hat{\phi})}{\hat{\phi}} \frac{d\hat{\theta}_\pm}{d\hat{\phi}}(\hat{\phi}). \tag{4.16}$$

The lens equation (4.2) has symmetry with respect to the point $\hat{\phi} = \hat{\theta} = 0$, so that

$$\hat{\theta}_-(\hat{\phi}) = -\hat{\theta}_+(-\hat{\phi}) \tag{4.17}$$

and

$$\frac{d\hat{\theta}_-}{d\hat{\phi}}(\hat{\phi}) = \frac{d\hat{\theta}_+}{d\hat{\phi}}(-\hat{\phi}). \tag{4.18}$$

Thus, the relation of the magnifications is given by

$$\mu_{0-}(\hat{\phi}) = \frac{\hat{\theta}_-(\hat{\phi})}{\hat{\phi}} \frac{d\hat{\theta}_-}{d\hat{\phi}}(\hat{\phi}) = \frac{\hat{\theta}_+(-\hat{\phi})}{-\hat{\phi}} \frac{d\hat{\theta}_+}{d\hat{\phi}}(-\hat{\phi}) = \mu_{0+}(-\hat{\phi}). \tag{4.19}$$

From the lens equation (4.2), we obtain

$$\mu_{0\pm} = \frac{\hat{\theta}_\pm^{2n+2}}{(\hat{\theta}_\pm^{n+1} \mp 1)(\hat{\theta}_\pm^{n+1} \pm n)}. \tag{4.20}$$

For $\hat{\phi} \gg 1$, Eq. (4.20) implies that $\mu_{0+} \simeq 1$ because $\theta_+ \simeq \hat{\phi} \gg 1$, while $\mu_{0-} \ll 1$ because $\theta_- \ll 1$. In other words, if it is far from the alignment, the positive image is as luminous as the unlensed image, while the negative image is extremely faint. Thus, we can ignore the gravitational lensing effects and the signed magnification sum $\mu_{0+} + \mu_{0-}$ becomes almost unity for $\hat{\phi} \gg 1$ regardless of the values of n.

4.2 Directly aligned limit

In this section we will discuss the signed magnification sums of the general spherical lens model for $n \geqq 1$ in the directly aligned limit ($\hat{\phi} \simeq 0$).

The positive image angle and magnification in the directly aligned limit ($\hat{\phi} \simeq 0$) are given by

$$\hat{\theta}_+(\hat{\phi}) \simeq 1 + \frac{1}{1+n}\hat{\phi} + \frac{n}{2(1+n)^2}\hat{\phi}^2 \tag{4.21}$$

and

$$\mu_{0+}(\hat{\phi}) \simeq \frac{1}{1+n}\frac{1+\hat{\phi}}{\hat{\phi}}, \tag{4.22}$$

respectively. From the symmetry, we can easily obtain the negative image angle and the signed magnification in the directly aligned limit

$$\hat{\theta}_{-}(\hat{\phi}) \simeq -1 + \frac{1}{1+n}\hat{\phi} - \frac{n}{2(1+n)^2}\hat{\phi}^2 \tag{4.23}$$

and

$$\mu_{0-}(\hat{\phi}) \simeq -\frac{1}{1+n}\frac{1-\hat{\phi}}{\hat{\phi}}, \tag{4.24}$$

respectively. Therefore the total magnification and the ratio of the magnifications in the directly aligned limit are given by

$$\mu_0(\hat{\phi}) \equiv \left|\mu_{0+}(\hat{\phi})\right| + \left|\mu_{0-}(\hat{\phi})\right| \simeq \frac{2}{1+n}\frac{1}{\hat{\phi}} \tag{4.25}$$

and

$$\left|\frac{\mu_{0+}(\hat{\phi})}{\mu_{0-}(\hat{\phi})}\right| \simeq \frac{1+\hat{\phi}}{1-\hat{\phi}}, \tag{4.26}$$

respectively.

The difference of the reduced image angle in the directly aligned limit is given by

$$\hat{\theta}_{+} - \hat{\theta}_{-} \simeq 2 + \frac{n}{(1+n)^2}\hat{\phi}^2. \tag{4.27}$$

Thus, the Einstein ring angle is given by

$$\theta_0 \simeq \frac{(1+n)^2(\theta_{+} - \theta_{-})}{2(1+n)^2 + n\hat{\phi}^2} \tag{4.28}$$

in terms of $\theta_{+} - \theta_{-}$ and $\hat{\phi}$.

Chapter 5

Gravitational lenses in the strong field limit

In this chapter, we will review and investigate gravitational lenses on the spherically symmetric and static spacetime in the strong field limit. Gravitational lensing is on the strong field has been investigated eagerly for the Schwarzschild black hole [21, 22, 23, 24, 27, 28, 30, 31, 55, 91, 92, 93, 94, 95], the Kerr black hole [96, 97, 98], the Reissner-Nordstrom black hole [31, 91, 94, 95, 99], the Gibbons-Maeda-Garfinkle-Horowitz-Strominger charged black hole [100], Einstein-Born-Infeld black holes [94, 101], braneworld black holes [47, 48, 102, 103], a static spherically symmetric spacetime of Brans-Dicke scalar-tensor theory [104], naked singularities [23, 29], the Janis-Newman-Winicour solution [16, 31, 94, 95], the Barriola-Vilenkin monopole [33], and wormholes [14, 16, 33, 87] because it can give clues for verification of gravitational theory in the strong filed. In Sec. 5.1, we review the magnification and the radii of relativistic images in the strong field limit [30, 31]. In Sec. 5.2, we review gravitational lensing in the strong field limit on the Schwarzschild spacetime in brief [30, 31] and in Sec. 5.3, we investigate gravitational lensing in the strong field limit on the Ellis wormhole spacetime.

5.1 Bozza's analysis

We briefly review Bozza's analysis of the magnification and the angles of relativistic images [30, 31]. We consider that the deflection angle of the light in the strong field limit is written by

$$\alpha(\theta) = -\bar{a} \log \left(\frac{\theta D_l}{b_c} - 1 \right) + \bar{b} + O(\theta D_l - b_c), \tag{5.1}$$

where b_c is the critical impact parameter, $\bar{a}$ is a positive parameter and $\bar{b}$ is a regular parameter. We will calculate the parameters $\bar{a}$ and $\bar{b}$ for the Schwarzschild lens and the Ellis wormhole in Sec. 5.2 and Sec 5.3, respectively.

When the winding number $n \geq 1$, we define an angle $\theta^0_{n\geq1}$ by

$$\alpha(\theta^0_{n\geq1}) = 2\pi n. \tag{5.2}$$

From Eqs. (5.1) and (5.2), we obtain

$$\theta^0_{n\geq1} = \frac{b_c}{D_l}(1 + e^{\frac{\bar{b}-2\pi n}{\bar{a}}}). \tag{5.3}$$

We expand the deflection angle $\alpha(\theta)$ around $\theta = \theta^0_{n\geq1}$ to obtain the effective deflection angle $\bar{\alpha}$. We define the small angle

$$\Delta\theta_{n\geq1} \equiv \theta_{n\geq1} - \theta^0_{n\geq1}, \tag{5.4}$$

where $\theta_{n\geq1}$ is the solution of the lens equation (2.1) with the winding number $n \geq 1$. From Eqs. (5.1) and (5.3), the effective deflection angle of the light in the strong field limit is given by

$$\bar{\alpha} = -\frac{D_l}{b_c}\bar{a}e^{\frac{-\bar{b}+2\pi n}{\bar{a}}}\Delta\theta_{n\geq1}. \tag{5.5}$$

We substitute the effective deflection angle (5.5) into the lens equation (2.1) and obtain

$$\phi = \theta^0_{n\geq1} + \left(1 + \frac{D_l}{b_c}\bar{a}e^{\frac{-\bar{b}+2\pi n}{\bar{a}}}\frac{D_{ls}}{D_s}\right)\Delta\theta_{n\geq1}. \tag{5.6}$$

From Eqs. (5.6) and (5.4), We get the angles of the relativistic images $\theta_{n\geq1}$

$$\theta_{n\geq1} \simeq \theta^0_{n\geq1} + \frac{b_c}{D_l}\frac{e^{\frac{\bar{b}-2\pi n}{\bar{a}}}}{\bar{a}}\frac{D_s}{D_{ls}}\left(\phi - \theta^0_{n\geq1}\right), \tag{5.7}$$

where we have used $b_c/D_l \ll 1$.

The magnification $\mu_{n\geq1}$ of the relativistic image is obtained by

$$\mu_{n\geq1} \simeq \frac{\theta_{n\geq1}}{\phi}\left.\frac{d\theta_{n\geq1}}{d\phi}\right|_{\theta_{n\geq1}=\theta^0_{n\geq1}} \simeq \frac{1}{\phi}\frac{b_c^2}{D_l^2}\frac{\left(1+e^{\frac{\bar{b}-2\pi n}{\bar{a}}}\right)e^{\frac{\bar{b}-2\pi n}{\bar{a}}}}{\bar{a}}\frac{D_s}{D_{ls}}. \tag{5.8}$$

The sum of the magnifications of all the relativistic images is given by

$$\sum_{n=1}^{\infty}\mu_n \simeq \frac{1}{\phi}\frac{b_c^2}{D_l^2}\frac{1}{\bar{a}}\frac{D_s}{D_{ls}}\frac{e^{\frac{\bar{b}}{\bar{a}}}}{e^{\frac{4\pi}{\bar{a}}}-1}\left(e^{\frac{2\pi}{\bar{a}}} + 1 + e^{\frac{\bar{b}}{\bar{a}}}\right) \tag{5.9}$$

and the sum of the magnifications of the relativistic images excluding the outermost relativistic image is given by

$$\sum_{n=2}^{\infty} \mu_n \simeq \frac{1}{\phi} \frac{b_c^2}{D_l^2} \frac{1}{\bar{a}} \frac{D_s}{D_{ls}} \frac{e^{\frac{\bar{b}-4\pi}{\bar{a}}}}{e^{\frac{4\pi}{\bar{a}}} - 1} \left(e^{\frac{4\pi}{\bar{a}}} + e^{\frac{2\pi}{\bar{a}}} + e^{\frac{\bar{b}}{\bar{a}}} \right). \tag{5.10}$$

From Eqs. (5.10) and (5.8), the ratio of the magnification of the outermost relativistic image divided by the sum of the magnification of the other relativistic images is given by

$$\frac{\mu_1}{\sum_{n=2}^{\infty} \mu_n} \simeq \frac{\left(e^{\frac{4\pi}{\bar{a}}} - 1 \right) \left(e^{\frac{2\pi}{\bar{a}}} + e^{\frac{\bar{b}}{\bar{a}}} \right)}{e^{\frac{4\pi}{\bar{a}}} + e^{\frac{2\pi}{\bar{a}}} + e^{\frac{\bar{b}}{\bar{a}}}} \simeq e^{\frac{2\pi}{\bar{a}}}. \tag{5.11}$$

From Eqs. (5.3) and (5.7), the innermost relativistic image angle is obtained by

$$\theta_\infty = \theta_\infty^0 = \frac{b_c}{D_l}. \tag{5.12}$$

From Eqs. (5.3), (5.7) and (5.12), the difference of the angles between the outermost relativistic image and innermost one is given by

$$\theta_1 - \theta_\infty \simeq \theta_1^0 - \theta_\infty = \theta_\infty e^{\frac{\bar{b}-2\pi}{\bar{a}}}. \tag{5.13}$$

Here, we ignored the second term of the right-hand side of the Eq. (5.7).

5.2 Strong field limit in the Schwarzschild spacetime

In this section, we consider the strong field limit in the Schwarzschild spacetime [30, 31]. We use the trajectory equation of the photon (2.3) with the metric tensor (2.2). From Eq. (2.13), the deflection angle α is given by

$$\alpha = I(r_+) - \pi, \tag{5.14}$$

where

$$I(r_+) \equiv 2 \int_{r_+}^{\infty} \frac{dr}{r^2 \sqrt{G(r, r_+)}}, \tag{5.15}$$

where r_+ is the closest distance of the photon orbit and

$$G(r, r_+) \equiv \frac{1}{r_+^2} \left(1 - \frac{r_g}{r_+} \right) + \frac{1}{r^2} \left(-1 + \frac{r_g}{r} \right). \tag{5.16}$$

Using

$$z \equiv 1 - \frac{r_+}{r}, \tag{5.17}$$

The integral $I(r_+)$ is obtained by

$$I(r_+) = 2\int_0^1 f(z, r_+) dz, \tag{5.18}$$

where

$$\begin{aligned} f(z, r_+) &\equiv \frac{1}{\sqrt{r_+^2 G(z, r_+)}} \\ &= \frac{1}{\sqrt{1 - \frac{r_g}{r_+} + (1-z)^2 \left[-1 + \frac{r_g}{r_+}(1-z)\right]}}. \end{aligned} \tag{5.19}$$

We will divide the integral $I(r_+)$ into the divergent part $I_D(r_+)$ and the regular part $I_R(r_+)$, or

$$I(r_+) = I_D(r_+) + I_R(r_+). \tag{5.20}$$

The divergent part $I_D(r_+)$ is defined by

$$I_D(r_+) \equiv 2\int_0^1 f_0(z, r_+) dz, \tag{5.21}$$

where

$$f_0(z, r_+) \equiv \frac{1}{\sqrt{\kappa(r_+) z + \beta(r_+) z^2}}, \tag{5.22}$$

where

$$\kappa(r_+) \equiv 2 - \frac{3r_g}{r_+}, \tag{5.23}$$

$$\beta(r_+) \equiv -1 + \frac{3r_g}{r_+}. \tag{5.24}$$

The divergent part $I_D(r_+)$ is calculated in a straight way and obtained by

$$\begin{aligned} I_D(r_+) &= \frac{2}{\sqrt{\beta(r_+)}} \log \left| \frac{\kappa(r_+) + 2\beta(r_+) + 2\sqrt{(\kappa(r_+) + \beta(r_+))\beta(r_+)}}{\kappa(r_+)} \right| \\ &= \frac{4}{\sqrt{\beta(r_+)}} \log \left(\frac{\sqrt{\beta(r_+)} + \sqrt{\kappa(r_+) + \beta(r_+)}}{\sqrt{\kappa(r_+)}} \right). \end{aligned} \tag{5.25}$$

Thus, the divergent part $I_D(r_+)$ in the strong field limit $r_+ \to 3r_g/2 + 0$ is obtained by

$$I_D(r_+) = -2\log\left(\frac{2r_+}{3r_g} - 1\right) + 2\log 2 + O\left(r_+ - \frac{3r_g}{2}\right). \tag{5.26}$$

From the relation between the impact parameter b and the closest distance r_+ (2.12), it follows that

$$\log\left(\frac{2r_+}{3r_g} - 1\right) = \frac{1}{2}\log\left(\frac{2b}{3\sqrt{3}r_g} - 1\right) + \frac{1}{2}\log\left(\frac{2}{3}\right). \tag{5.27}$$

Thus, the divergent part $I_D(b)$ in the strong field limit $b \to \frac{3\sqrt{3}r_g}{2} + 0$ is obtained by

$$I_D(b) = -\log\left(\frac{2b}{3\sqrt{3}r_g} - 1\right) + \log 6 + O\left(b - \frac{3\sqrt{3}r_g}{2}\right). \tag{5.28}$$

The regular part $I_R(r_+)$ is defined by

$$I_R(r_+) \equiv \int_0^1 g(z, r_+)dz, \tag{5.29}$$

where

$$g(z, r_+) \equiv f(z, r_+) - f_0(z, r_+). \tag{5.30}$$

In the strong field limit $r_+ \to 3r_g/2 + 0$, the regular part $I_R(r_+)$ becomes

$$\begin{aligned} I_R(r_+) &= 2\int_0^1 \left(\frac{1}{z\sqrt{1 - \frac{2}{3}z}} - \frac{1}{z}\right) dz + O\left(r_+ - \frac{3r_g}{2}\right) \\ &= 2\log\left[6\left(2 - \sqrt{3}\right)\right] + O\left(r_+ - \frac{3r_g}{2}\right). \end{aligned} \tag{5.31}$$

Thus, the deflection angle of the light on the Schwarzschild spacetime in the strong field limit is obtained by

$$\begin{aligned} \alpha(\theta) &= I_D + I_R - \pi \\ &= -\log\left(\frac{2\theta D_l}{3\sqrt{3}r_g} - 1\right) + \log\left[216\left(7 - 4\sqrt{3}\right)\right] - \pi + O\left(\theta D_l - \frac{3\sqrt{3}r_g}{2}\right) \end{aligned} \tag{5.32}$$

where we have used the image angle $\theta = b/D_l$ and we get the parameters $\bar{a} = 1$ and $\bar{b} = \log\left[216\left(7 - 4\sqrt{3}\right)\right] - \pi \simeq -0.40$.

The magnification of all the relativistic images on the Schwarzschild spacetime is obtained by

$$\sum_{n=1}^{\infty} \mu_n \simeq \frac{1}{\phi}\frac{27}{4}\left(\frac{r_g}{D_l}\right)^2 \frac{D_s}{D_{ls}} e^{\bar{b}-2\pi} = \frac{1}{\phi}\frac{27}{16}\theta_0^4 \left(\frac{D_s}{D_{ls}}\right)^3 e^{\bar{b}-2\pi}. \tag{5.33}$$

The ratio of the magnification of the weak field image divided by the sum of the magnification of all the relativistic images is given by

$$\frac{\mu_0}{\sum_{n=1}^{\infty}\mu_n} \simeq \frac{4\sqrt{2}}{27}\left(\frac{D_l}{r_g}\right)^{\frac{3}{2}}\left(\frac{D_{ls}}{D_s}\right)^{\frac{3}{2}} e^{2\pi-\bar{b}} = \frac{16}{27}\frac{1}{\theta_0^3}\left(\frac{D_{ls}}{D_s}\right)^3 e^{2\pi-\bar{b}} \gg 1. \tag{5.34}$$

Thus, we can ignore the effect of the relativistic images on the light curve in the Schwarzschild spacetime. The ratio shows that the relativistic images are always fainter than images in the weak field. However, this does not mean that we cannot observe the relativistic images since they can get bright when the source angle is small. We may measure the relativistic images of the galactic black hole of our Galaxy ($\simeq 20\mu$as) with interferometry instruments which are now under development [105, 106, 107, 108].

The sum of the magnification of all the relativistic images become unity when the source angle is

$$\phi \simeq \frac{27}{4}\left(\frac{r_g}{D_l}\right)^2 \frac{D_s}{D_{ls}} e^{\bar{b}-2\pi} = \frac{27}{16}\theta_0^4\left(\frac{D_s}{D_{ls}}\right)^3 e^{\bar{b}-2\pi}. \tag{5.35}$$

Note that the cross section of gravitational lensing with the galactic black hole in our Galaxy is very tiny because the Einstein ring angle is $\theta_0 \simeq 10^{-6}$.

5.3 Strong field limit in the Ellis spacetime

The deflection angle of the light on the Ellis wormhole spacetime in the strong field limit is given by

$$\alpha(\theta) = -\log\left(\frac{\theta D_l}{a} - 1\right) + 3\log 2 - \pi + O(\theta D_l - a). \tag{5.36}$$

Here, we have used the relation

$$\lim_{k\to 1} K(k) = \log\frac{4}{k'} + O(k'^2 \log k'), \tag{5.37}$$

where $k' = (1-k^2)^{\frac{1}{2}}$ and $0 < k < 1$. Therefore, $\bar{a} = 1$ and $\bar{b} = 3\log 2 - \pi$.

The magnification of the all relativistic images on the Ellis wormhole spacetime is obtained by

$$\sum_{n=1}^{\infty} \mu_n \simeq \frac{1}{\phi}\left(\frac{a}{D_l}\right)^2 \frac{D_s}{D_{ls}} e^{\bar{b}-2\pi} = \frac{4}{\pi}\frac{\theta_0^3}{\phi}\left(\frac{D_s}{D_{ls}}\right)^2 e^{\bar{b}-2\pi}. \tag{5.38}$$

The ratio of the magnification of the weak field image divided by the sum of the magnification of the all relativistic images is given by

$$\frac{\mu_0}{\sum_{n=1}^{\infty}\mu_n} \simeq \frac{2}{3}\left(\frac{\pi}{4}\right)^{\frac{1}{3}}\left(\frac{D_l}{a}\right)^{\frac{4}{3}}\left(\frac{D_{ls}}{D_s}\right)^{\frac{4}{3}} e^{2\pi-\bar{b}} = \frac{\pi}{6}\frac{1}{\theta_0^2}\left(\frac{D_{ls}}{D_s}\right)^2 e^{2\pi-\bar{b}} \gg 1 \tag{5.39}$$

Thus, we can also ignore the effect of the relativistic images on the light curve in the Ellis wormhole spacetime. The sum of the magnification of all the relativistic images become unity when the source angle is

$$\phi \simeq \left(\frac{a}{D_l}\right)^2 \frac{D_s}{D_{ls}} e^{\bar{b}-2\pi} = \frac{4}{\pi}\theta_0^3\left(\frac{D_s}{D_{ls}}\right)^2 e^{\bar{b}-2\pi}. \tag{5.40}$$

We notice that the cross section of the gravitational lensing in the strong field limit is different from the one in the Schwarzschild spacetime.

Chapter 6

Comparison of exotic lenses and mass lenses

In this chapter, we will investigate two new methods to distinguish between exotic matter objects and black holes with gravitational lenses. In Sec. 6.1, we compare the Einstein ring and the relativistic Einstein rings in the Ellis wormhole spacetime to the ones in the Schwarzschild spacetime and show that we can distinguish between black holes and wormholes. In Sec. 6.2, we show that we can distinguish between mass lenses and exotic matter objects with their signed magnifications.

6.1 Comparison the Einstein ring systems

In this section we compare the Einstein ring and the relativistic Einstein rings in the Ellis wormhole spacetime to the ones in the Schwarzschild spacetime and show that we can distinguish between black holes and wormholes.

The Einstein ring and the relativistic Einstein ring images correspond to the the solution θ_n of the lens equation (2.1) with the winding number n for vanishing source angle $\phi = 0$.

First, we consider the Einstein ring and the relativistic Einstein rings on the Ellis wormhole spacetime. From the lens equation (2.1), the deflection angle (3.84) and $b = D_l\theta$, we find that the ring image is given by

$$\theta_n = \frac{a}{D_l}\frac{1}{k_n}, \tag{6.1}$$

where $k_n \in (0, 1)$ is a unique root of the transcendental equation

$$2K(k) - \frac{\eta}{k} = (2n + 1)\,\pi, \tag{6.2}$$

where $\eta \equiv D_s a/(D_l D_{ls})$ and $k \equiv a/b$.

We should note that $2K(k) - \eta/k$ is monotonically increasing with respect to k and changes from $-\infty$ to ∞ as k increases from 0 to 1. The uniqueness of the root follows from the monotonicity. Moreover, we can conclude that k_n monotonically increases and approaches 1 as $n \to \infty$ and hence the image angle θ_n monotonically decreases and approaches a/D_l.

In the weak-field regime $|b| \gg a$, the winding number n should be $n = 0$. Using the deflection angle (3.86), we can solve the transcendental equation (6.2) approximately and get the diameter angle of the Einstein ring

$$\begin{aligned}\theta_0 &\simeq \left(\frac{\pi}{4}\frac{D_{ls}}{D_s D_l^2}a^2\right)^{\frac{1}{3}} \\ &\simeq 2.0\,\text{arcseconds}\left(\frac{D_{ls}}{10\text{Mpc}}\right)^{\frac{1}{3}}\left(\frac{20\text{Mpc}}{D_s}\right)^{\frac{1}{3}}\left(\frac{10\text{Mpc}}{D_l}\right)^{\frac{2}{3}}\left(\frac{a}{0.5\text{pc}}\right)^{\frac{2}{3}}. \quad (6.3)\end{aligned}$$

This approximation is good for $D_l \gg a$ and $D_{ls} \gg a$. The relative error is $\simeq 10^{-2}$ for $a = 0.5$pc and $D_l = D_{ls} = 10$ Mpc.

In the especially strong-field regime, where the winding number n becomes $n \geq 1$, we can easily check that $a \simeq b$ or $k_n \simeq 1$ satisfies the transcendental equation (6.2) in numerical calculations. Physically this means that the light rays which wind around the wormhole nearly on the photon sphere make the relativistic Einstein rings [31, 33]. Then the diameter angles of the relativistic Einstein rings are approximately given by

$$\begin{aligned}\theta_{n\geq 1} &\simeq \frac{a}{D_l} \\ &\simeq 1.0 \times 10^{-2}\,\text{arcseconds}\left(\frac{10\text{Mpc}}{D_l}\right)\left(\frac{a}{0.5\text{pc}}\right). \quad (6.4)\end{aligned}$$

Regardless of the values of D_{ls}, D_l and a, the relative error of the above approximation to the direct numerical solution of the outermost relativistic Einstein ring ($n = 1$) is $\simeq 10^{-3}$ and those of the other relativistic Einstein rings ($n \geq 2$) are smaller than 10^{-5}. This implies that it is difficult to resolve each relativistic Einstein ring separately.

Thus, we conclude that there are one Einstein ring image and countably infinite relativistic Einstein ring images, the latter of which accumulate to form the apparently single ring image of the throat with the diameter a/D_l. This conclusion does not depend on the value of η.

If we are given the distance D_s to the source from the observer, the distance D_l to the lens from the observer and the radius θ_0 of the Einstein ring, we can determine the radius of the throat a from Eq. (6.3). Then, we can use $\theta_{n\geq1}$ (6.4) to test the assumption that the lens object is a wormhole.

From Eqs. (6.3) and (6.4) we obtain the relation between θ_0 and $\theta_{n\geq1}$ by

$$\theta_{n\geq1} \simeq \left(\frac{4}{\pi}\frac{D_s}{D_{ls}}\right)^{\frac{1}{2}} \theta_0^{\frac{3}{2}}. \tag{6.5}$$

This relation generally holds in astrophysical situations, as long as $a \ll D_l$ and $a \ll D_{ls}$ are satisfied.

Second, we consider the Einstein ring and the relativistic Einstein rings on the Schwarzschild spacetime.

In the weak-field regime $b \gg r_g$, the winding number n should vanish and the deflection angle is given by $\alpha \simeq 2r_g/b$. See Eq. (2.22). From the deflection angle (2.22) and the lens equation (2.1), the diameter angle of the Einstein ring is given by

$$\begin{aligned}\theta_0 &\simeq \sqrt{\frac{2D_{ls}}{D_l D_s} r_g} \\ &\simeq 2.0\,\text{arcseconds} \left(\frac{D_{ls}}{10\text{Mpc}}\right)^{\frac{1}{2}} \left(\frac{M}{10^{10}M_\odot}\right)^{\frac{1}{2}} \left(\frac{10\text{Mpc}}{D_l}\right)^{\frac{1}{2}} \left(\frac{20\text{Mpc}}{D_s}\right)^{\frac{1}{2}}. \end{aligned} \tag{6.6}$$

We can determine r_g in the same way as the radius of the throat a.

In the especially strong-field regime, where the winding number n becomes $n \geq 1$, the impact parameter b that satisfies the lens equation should be nearly the critical impact parameter $b_c = (3\sqrt{3}/2)r_g$ (see [28, 30, 31]). Then the diameter angles of the inseparable relativistic Einstein rings $\theta_{n\geq1}$ are given by

$$\begin{aligned}\theta_{n\geq1} &\simeq \frac{3\sqrt{3}}{2}\frac{r_g}{D_l} \\ &\simeq 5.1 \times 10^{-5}\,\text{arcseconds} \left(\frac{M}{10^{10}M_\odot}\right) \left(\frac{10\text{Mpc}}{D_l}\right). \end{aligned} \tag{6.7}$$

Regardless of the values of D_{ls}, D_l and r_g, the relative error of the above approximation to the direct numerical solution of the outermost relativistic Einstein ring ($n = 1$) is $\simeq 10^{-3}$ and those of the other relativistic Einstein rings ($n \geq 2$) are smaller than 10^{-5}.

It is useful to remember that the leading term of the deflection angle in the weak-field regime is the second order of the small amount a/b on the Ellis wormhole geometry (3.86), while it is the first order of the small amount r_g/b on the Schwarzschild geometry (2.22). So the relation between θ_0 and $\theta_{n\geq1}$ for the Schwarzschild spacetime

$$\theta_{n\geq1} \simeq \frac{3\sqrt{3}}{4}\frac{D_s}{D_{ls}}\theta_0^2 \tag{6.8}$$

is different from that on the Ellis wormhole spacetime (6.5). Figure 6.1 shows the angle of the relativistic Einstein ring $\theta_{n\geq 1}$ versus the angle of the Einstein ring θ_0 for $D_l = D_{ls} = 10\text{Mpc}$. Thus, we can distinguish between black holes and wormholes in principle if we are given D_s/D_l, θ_0 and $\theta_{n\geq 1}$.

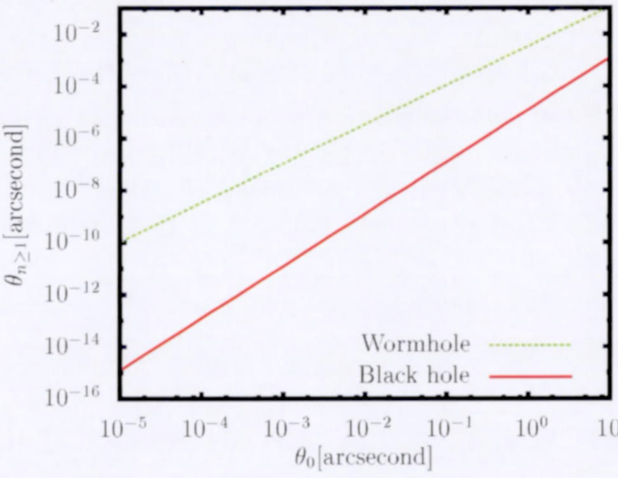

Figure 6.1: The angle of the relativistic Einstein ring $\theta_{n\geq 1}$ versus the angle of the Einstein ring θ_0 for $D_l = D_{ls} = 10\text{Mpc}$. The broken (green) and solid (red) lines plot the cases where the lens objects are a wormhole and a black hole, respectively. This figure is taken from [52].

6.2 Comparison of the signed magnification sums

In this section, we show that we can distinguish between mass lenses and exotic matter objects with their signed magnifications.

Figure 6.2 shows that one can distinguish the general spherical lens models with their signed magnification sums $\mu_{0+} + \mu_{0-}$ which are less than unity. We also can see that one can distinguish the general spherical lens with $n = 1$ from $n = 2$, 3 and 4 but one cannot distinguish between $n = 2$, 3 and 4 for $\hat{\phi} \gtrsim 2$.

Note that we have to know the unlensed luminosity to calculate the signed magnification sum $\mu_{0+} + \mu_{0-}$. If we observe a double lensed image with $\hat{\phi} \gtrsim 2$ and the unlensed image with $\hat{\phi} \gg 1$, we can obtain the the signed magnification sum $\mu_{0+} + \mu_{0-}$. We also can see that one can distinguish $n = 1$

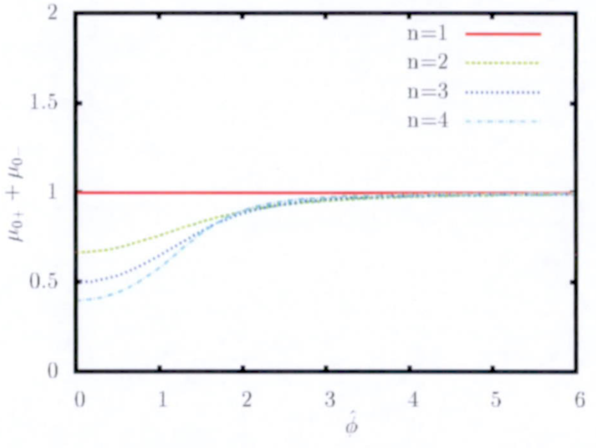

Figure 6.2: The signed magnification sums of some general spherical lens models. The solid, broken, dot and dot-dashed lines are the general spherical lens models for $n = 1$, 2, 3 and 4, respectively. This shows that the signed magnification sums is a useful tool to detect the exotic objects with $n > 1$. This figure is taken from [90].

from $n = 2$, 3 and 4 but one cannot distinguish between $n = 2$, 3 and 4 for $\hat{\phi} \gtrsim 2$. The minimum value of the signed magnification sums is given by, from Eqs. (4.22) and (4.24),

$$\lim_{\hat{\phi}\to 0}\left(\mu_{0+}(\hat{\phi}) + \mu_{0-}(\hat{\phi})\right) = \frac{2}{1+n}. \tag{6.9}$$

The lower bound of the total magnification μ_0 is given by

$$\frac{2}{1+n} \leq \mu_{0+} + \mu_{0-} \leq |\mu_{0+}| + |\mu_{0-}| = \mu_0. \tag{6.10}$$

Therefore, gravitational lensing necessarily gives amplified light curves for $n = 1$, while it does not necessarily for $n > 1$ (see Appendix B for microlensing).

For $n = 0$ these analyses are not valid in the region $1 < \hat{\phi}$ because of the non-existence of the negative image angle $\hat{\theta}_-$ as discussed in the chapter 4. However, it is valid in the region $0 \leq \hat{\phi} \leq 1$. For $1 < \hat{\phi}$, the magnification is

$$1 \leq \mu_{0+}(\hat{\phi}) \leq 2. \tag{6.11}$$

and the total magnification $\mu_{0+}(\hat{\phi}) + \mu_{0-}(\hat{\phi})$ is always 2 in the range $0 \leq \hat{\phi} \leq 1$. So one can also distinguish the case $n = 0$ from the other cases.

Chapter 7

Discussion and Conclusion

Einstein ring systems

It is understood that the qualitative features of the gravitational lensing on the Ellis wormhole spacetime are very similar to the ones on the Schwarzschild spacetime for their photon spheres and their asymptotic flatness [14, 33, 87]. However, we realize that their quantitative features are very different due to their different weak-field behaviors.

We consider the experimental situation where we know the separation D_s between the observer and the source and the separation D_l between the observer and the lens. We assume that we do not know whether the lens object is a black bole or a wormhole and do not its parameter, i.e., the mass M or the radius a of the throat in advance.

We need at least two observable quantities to determine whether the lens object is a black hole or wormhole since the lens system has one parameter in this situation. First, we observe an Einstein ring and determine the parameter for both possibilities. Second, we observe relativistic Einstein rings and tell the wormhole from the black hole. If the predicted relativistic ring angles by the black hole and by the wormhole were of similar size, we could not discern the difference. However, Eqs. (6.5) and (6.8) and Fig. 6.1 show that we do not confuse them.

We conclude that we can detect the relativistic Einstein rings by wormholes which have $a \simeq 0.5$pc at a galactic center with the distance $D_l = D_{ls} = 10$Mpc and which have $a \simeq 10$AU in our galaxy with the distance $D_l = D_{ls} = 10$kpc using the most powerful modern instruments which have the resolution of 10^{-2}arcseconds such as a 10-meter optical-infrared telescope. Note that the corresponding black holes which have the Einstein rings of the same size are galactic supermassive black holes with $10^{10}M_\odot$ and $10^7M_\odot$, respectively, and that the relativistic Einstein rings by these black holes are too small to measure with the current technology.

In fact, our results imply that we can distinguish between slowly rotating Kerr-Newman black holes and the Ellis wormholes with their Einstein ring systems. This is because the leading term of the deflection angle for the lensing by the Kerr-Newman black holes in the weak-field regime is equal to the one for the lensing by the Schwarzschild black holes, while the black hole charge and small spin only slightly change the radii of the relativistic Einstein rings [31, 96, 99, 109, 110]. Moreover, this also suggests that it is much more challenging to determine the charge and/or small spin of black holes than to distinguish between black holes and the Ellis wormholes.

We assumed that the observer, the lensing object and the source object are directly-aligned, though such a configuration is fairly rare. In general the strong gravitational lensing effect is observed as broken-ring images which are called relativistic images [28]. Therefore, more realistic problem is to size the relativistic images. Our result suggests that we can distinguish black holes and wormholes by using the relativistic images. To observe the relativistic images is one of the challenging works with many difficulties. Bozza *et al.* pointed out that relativistic images are always very faint with respect to the weak field images [30]. The Very Large Telescope Interferometer (VLTI) has high resolution [111, 112] but it will not work because of this demagnifying effect.

We also assumed point-like sources, although astrophysical sources have their own size. If the source object is a galaxy, it may conceal the relativistic Einstein rings, especially, in the case where the lens object is a black hole. Testing some hypotheses of astrophysical wormholes by using the relativistic Einstein rings and the Einstein ring is left as future work.

Tejeiro and Larranaga [87] investigated the gravitational lensing effect of the wormhole solution obtained by connecting the Ellis wormhole solution as an interior region and the Schwarzschild solution as an exterior region [113]. They concluded that we cannot distinguish the Schwarzschild black hole and the wormhole unless the discontinuity of the magnification curve at the boundary is observed. This does not contradict our results because their wormhole solution behaves as the Schwarzschild solution in the weak-field regime.

Signed magnification sums

It is well known that the signed magnification sum of the Schwarzschild lens is always unity in the weak field limit. We realize that one can distinguish the exotic lenses with the parameter $n > 1$ of the general spherical lens such as Ellis wormhole from mass lens systems because the signed magnification sums of exotic lenses are less than unity.

The signed magnification sum is a powerful tool to find exotic lens objects because it only depends on the reduced source angle $\hat{\phi}$ and n and we just have to observe the images for $\hat{\phi} \lesssim 1$ and for $\hat{\phi} \gg 1$ to determine the signed magnification sum. However, we need a high resolution to observe the double images. We would also distinguish the lens objects with the ratio of magnifications of the double images and the total magnification. If we also measure the difference $\theta_+ - \theta_-$ of the image angles, one can determine the Einstein ring angle θ_0 and the source angle $\phi = \theta_0\hat{\phi}$.

Observing double lensed images is a practical idea to search the exotic lenses. Over than a hundred strong lensing including many double images have been found so far [49]. Future surveys by Pan-Starrs [114], Dark Energy Survey [115], Subaru Hyper Suprime-Cam [116] and Large Synoptic Survey Telescope [50] will find more multiple images of lensed quasars. These surveys will give the stricter upper bound of the number density for wormholes or detect wormholes.

The method to detect the Ellis wormholes and other exotic lenses by observing the light curves with the characteristic demagnification by Abe [88] and Kitamura *et al.* [117]. Notice that the method to distinguish the lens objects with the signed magnification sums would be used in both the magnification and demagnification phases. Thus, we do not have to rely on only the demagnification to detect the Ellis wormholes and other exotic lenses.

Our method with the signed magnification sums is complementary to the methods to detect exotic lens objects with the light curves [88, 117] and the astrometric image centroid displacements [89].

In this thesis, we only consider gravitational lensing effects of the simplest wormhole. Analyses of gravitational lensing effects by most wormhole solutions which have been found thus far are left as future works.

Appendix A

Magnification in the Reissner-Nordstrom spacetime

In this appendix, we consider the Reissner-Nordstrom Black hole which is a black hole solution with the electrical charge.[99, 109, 118] The line element of the Reissner-Nordstrom spacetime is given by

$$\begin{aligned} ds^2 &= -\left(1-\frac{2M}{r}+\frac{Q^2}{r^2}\right)dt^2+\left(1-\frac{2M}{r}+\frac{Q^2}{r^2}\right)^{-1}dr^2 \\ &\quad +r^2(\sin^2\Theta d\Phi^2+d\Theta^2). \end{aligned} \tag{A.1}$$

We consider the weak field approximation. If the amount of the charge is small $Q/M \le 1$, the metric is given by, in the quasi-Minkowskian coordinates t and $\boldsymbol{X}$,

$$\begin{aligned} ds^2 &\simeq -\left[1-\frac{2M}{X}+\left(1+\frac{1}{2}\frac{Q^2}{M^2}\right)\frac{2M^2}{X^2}\right]dt^2 \\ &\quad +\left[1+\frac{2M}{X}+\left(1-\frac{1}{3}\frac{Q^2}{M^2}\right)\frac{3M^2}{2X^2}\right]d\boldsymbol{X}^2. \end{aligned} \tag{A.2}$$

The deflection angle α in the weak field limit is given by

$$\alpha = \frac{4M}{b}+\frac{3\pi}{4}\left(5-\frac{Q^2}{M^2}\right)\frac{M^2}{b\,|b|}, \tag{A.3}$$

where b is the impact parameter of the photon. The signed magnifications $\mu_{0\pm}$ are given by

$$\mu_{0\pm} = \frac{1}{2}-\frac{3\pi}{32\left(\hat{\phi}^2+4\right)^{\frac{3}{2}}}\left(5-\frac{Q^2}{M^2}\right)\sqrt{\frac{MD_s}{D_l D_{ls}}}\pm\frac{\hat{\phi}^2+2}{2\hat{\phi}\sqrt{\hat{\phi}^2+4}}. \tag{A.4}$$

We see that we cannot detect the effect of the electrical charge with microlensing at $O(M^2/b^2)$ of the deflection angle α because of the cancelling [118].

Appendix B

Microlensing

In this appendix, we will review the microlensing of exotic lenses in brief [88, 117, 119]. We consider the situation that a lens object exists in our galaxy and a source goes across near the lens object on the lens plane. We define the smallest source angle as β_0. Figure B.1 shows the source trajectory with $\beta_0 \simeq 0.4\theta_0$ on the lens plane.

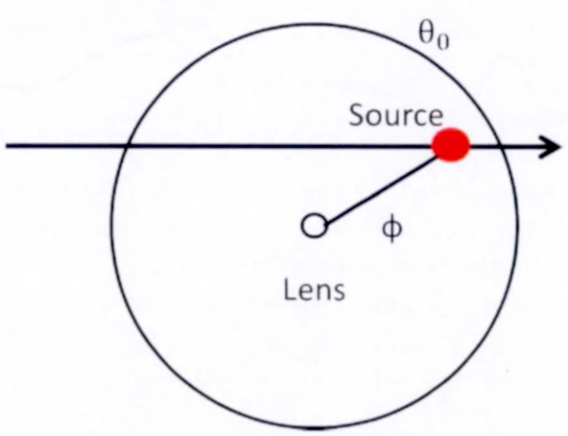

Figure B.1: A source trajectory on a lens plane with the smallest source angle $\beta_0 \simeq 0.4\theta_0$. The large circle expresses the Einstein ring angle.

Figure B.2 shows the light curves of the microlensing for the mass lens and the Ellis wormhole [88]. We realize that the Ellis wormhole lens shows the characteristic demagnification and the light curves is useful tool to detect the Ellis wormholes.

Figure B.3 shows the light curves for the general spherical lens with the reduced smallest source angle $\hat{\beta}_0 \equiv \beta_0/\theta_0 = 0.1$ [117]. We can determine n

from the characteristic dips.

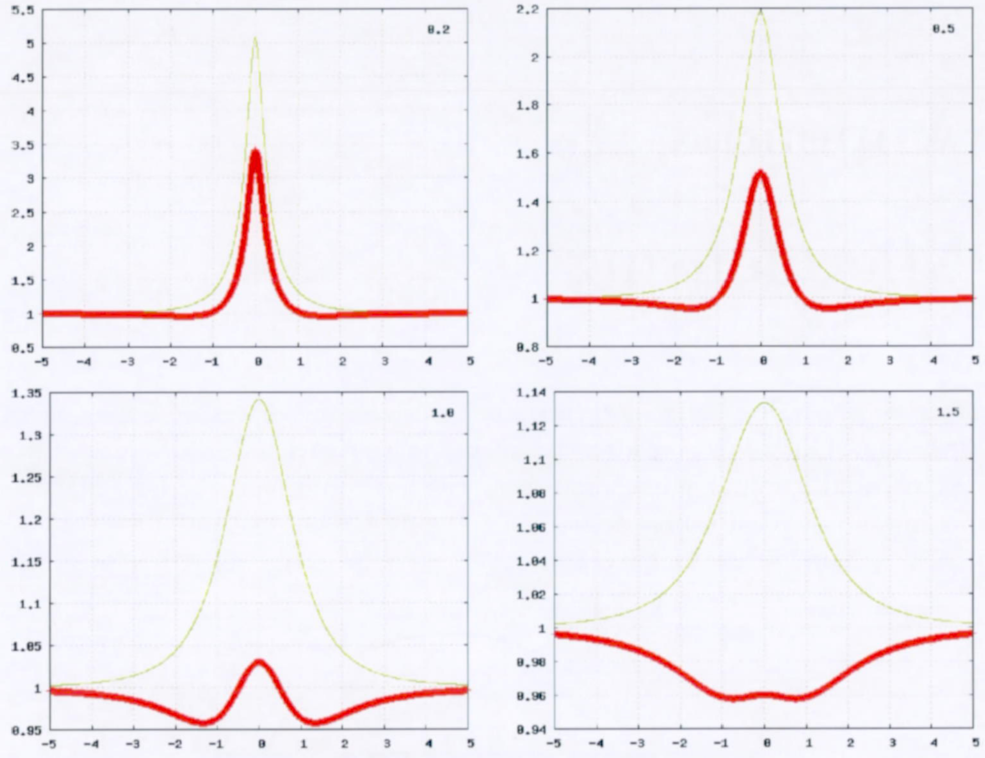

Figure B.2: The light curves for the $\beta_0 = 0.2\theta_0$ (top left), $\beta_0 = 0.5\theta_0$ (top right), $\beta_0 = 1.0\theta_0$ (bottom left) and $\beta_0 = 1.5\theta_0$ (bottom right). The thin (green) lines and the thick (red) lines, respectively, correspond to the mass lens and the Ellis wormhole lens. These figures are taken from [88].

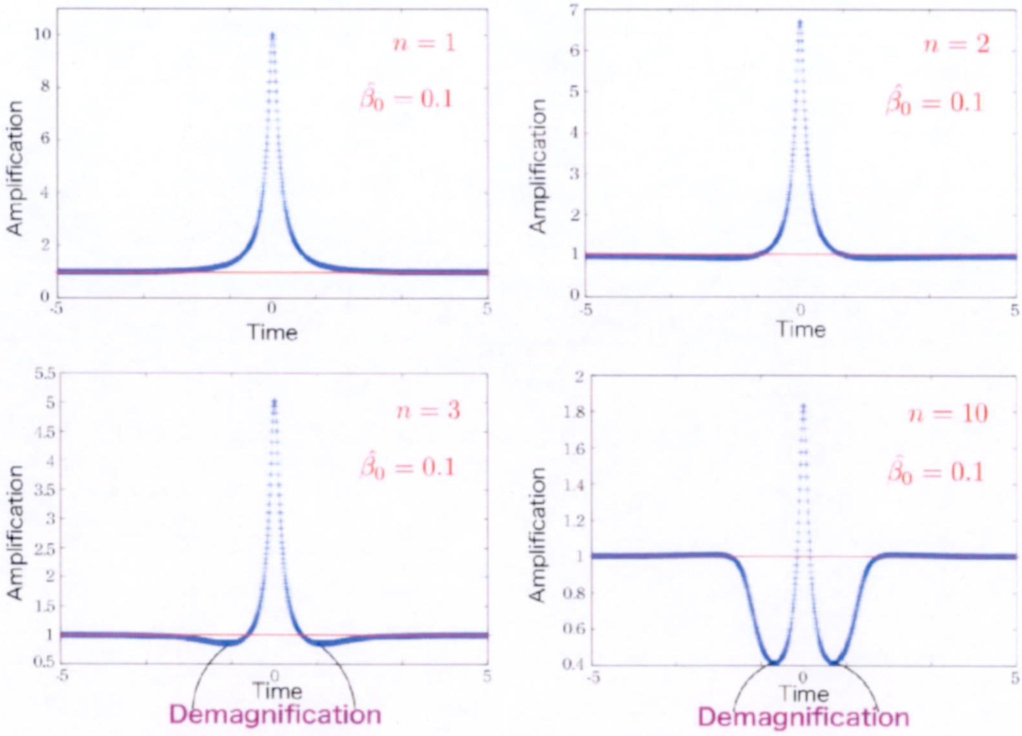

Figure B.3: The light curves for the general spherical lens with $n = 1$ (top left), $n = 2$ (top right), $n = 3$ (bottom left) and $n = 10$ (bottom right) for the reduced smallest source angle $\hat{\beta}_0 \equiv \beta_0/\theta_0 = 0.1$. These figures are taken from [117].

Appendix C

Bozza's analysis for the Ellis wormhole

Bozza calculated the deflection angle of the light on the static and spherical black holes spacetime with asymptotic flatness in the strong field limit and showed that some observable physical quantities are determined by the deflection angle in the strong field limit [31].

However, Bozza's calculation of the deflection angle of the light cannot directly be applied to the Ellis wormhole because Bozza's calculation does not work the ultra static coordinate. Nandi, Zhang and Zakharov might have used Bozza's calculation and get a wrong deflection angle in the strong field limit [14]. Their mistake affects measurable physical quantities such as the difference of the angles between outermost relativistic image and innermost one (5.13) and the ratio of the magnification of the outermost relativistic image divided by the sum of the magnification of the other relativistic images (5.11).

In this appendix, we will recalculate the deflection angle in the strong field limit in the Ellis wormhole spacetime on a similar way to Bozza's analysis.

The deflection angle α is then calculated to give

$$\alpha = I(b) - \pi, \tag{C.1}$$

where

$$I(b) \equiv 2\int_0^{b^{-1}} \frac{du}{\sqrt{G(u)}} \tag{C.2}$$

and

$$G(u) \equiv a^2(a^{-2} - u^2)(b^{-2} - u^2). \tag{C.3}$$

We transform

$$z = 1 - bu \tag{C.4}$$

and then

$$I(k) = \int_0^1 f(z,k)dz, \tag{C.5}$$

where

$$k \equiv \frac{a}{b} \tag{C.6}$$

and

$$f(z,k) \equiv \frac{2}{\sqrt{2(1-k^2)z + (-1+5k^2)z^2 - 4k^2z^3 + k^2z^4}}. \tag{C.7}$$

We divide $I(k)$ into the divergent part $I_D(k)$ and the regular part $I_R(k)$, or

$$I(k) = I_D(k) + I_R(k). \tag{C.8}$$

The divergent part $I_D(k)$ is defined by

$$I_D(k) \equiv \int_0^1 f_0(z,k)dz, \tag{C.9}$$

where

$$f_0(z,k) \equiv \frac{2}{\sqrt{\kappa z + \beta z^2}}, \tag{C.10}$$

$\kappa(k) \equiv 2(1-k^2)$ and $\beta(k) \equiv -1+5k^2$.

$\kappa(k)$ is always positive in the scattering case $(0 < k < 1)$. $\beta(k)$ is negative for $0 < k < 1/\sqrt{5}$, zero for $k = 1/\sqrt{5}$ and positive for $1/\sqrt{5} < k < 1$. Now we can concentrate in a strong field case $(1/\sqrt{5} < k < 1)$ where $\beta(k)$ should be positive because we will consider the strong field limit $(k \to 1)$. When both $\kappa(k)$ and $\beta(k)$ are positive, the divergent part $I_D(k)$ can be calculated [31],

$$\begin{aligned} I_D(k) &= \frac{4}{\sqrt{\beta}} \log \frac{\sqrt{\beta} + \sqrt{\kappa + \beta}}{\sqrt{\kappa}} \\ &= \frac{4}{\sqrt{-1+5k^2}} \log \frac{\sqrt{-1+5k^2} + \sqrt{1+3k^2}}{\sqrt{2(1-k)(k+1)}}. \end{aligned} \tag{C.11}$$

$\kappa(k)$ and $\beta(k)$ in the strong field limit yield,

$$\lim_{k\to 1} \kappa(k) = 0, \tag{C.12}$$

$$\lim_{k\to 1} \beta(k) = 4. \tag{C.13}$$

So, the divergent part $I_D(k)$ in the strong field limit is obtained by

$$I_D(k) = -\log(1-k) + 2\log 2 + O(k-1) \tag{C.14}$$

The regular part $I_R(k)$ is defined by

$$I_R(k) \equiv \int_0^1 g(z,k)dz, \tag{C.15}$$

where

$$g(z,k) \equiv f(z,k) - f_0(z,k). \tag{C.16}$$

We can expand $I_R(k)$ in powers of $(k-1)$,

$$I_R(k) = \sum_{n=0}^{\infty} \frac{1}{n!}(k-1)^n \int_0^1 \left.\frac{\partial^n g}{\partial k^n}\right|_{k=1} dz. \tag{C.17}$$

Now,

$$f_0(z,1) = \frac{1}{z}, \tag{C.18}$$

$$f(z,1) = \frac{2}{z(2-z)}, \tag{C.19}$$

$$\begin{aligned} g(z,1) &= f(z,1) - f_0(z,1) \\ &= \frac{1}{2-z}. \end{aligned} \tag{C.20}$$

So, the regular part $I_R(k)$ is

$$\begin{aligned} I_R(k) &= \int_0^1 g(z,1)dz + O(k-1) \\ &= \int_0^1 \frac{dz}{2-z} + O(k-1) \\ &= \log 2 + O(k-1). \end{aligned} \tag{C.21}$$

Thus, the deflection angle of the light on the Ellis wormhole spacetime in the strong field limit is obtained by

$$\begin{aligned} \alpha(k) &= I_D(k) + I_R(k) - \pi \\ &= -\log(1-k) + 3\log 2 - \pi + O(k-1). \end{aligned} \tag{C.22}$$

Since $b \simeq \theta D_l$,

$$\alpha(\theta) = -\log\left(\frac{\theta D_l}{a} - 1\right) + 3\log 2 - \pi + O(k-1). \tag{C.23}$$

Bibliography

[1] C. M. Will, *Theory and Experiment in Gravitational Physics*, (Cambridge University Press, Cambridge, England, 1993).

[2] Planck Collaboration, arXiv:1303.5076v1.

[3] P. Schneider, J. Ehlers and E. E. Falco, *Gravitational Lenses* (Springer-Verlag, Berlin, 1992).

[4] V. Perlick, Living Rev. Relativity **7**, 9 (2004), http://relativity.livingreviews.org/Articles/lrr-2004-9.

[5] V. Perlick, arXiv:1010.3416[gr-qc].

[6] A. O. Petters, H. Levine and J. Wambsganss, *Singularity Theory and Gravitational Lensing* (Birkhauser, Boston, 2001).

[7] M. Visser, *Lorentzian Wormholes: From Einstein to Hawking* (American Institute of Physics, Woodbury, NY, 1995).

[8] S. W. Kim and Y. M. Cho, in *Evolution of the Universe and its Observational Quest* (Universal Academy Press, Tokyo, 1994), p. 353.

[9] J. G. Cramer, R. L. Forward, M. S. Morris, M. Visser, G. Benford and G. A. Landis, Phys.Rev. D **51**, 3117 (1995).

[10] M. Safonova, D. F. Torres and G. E. Romero, Mod. Phys. Lett. A **16**, 153 (2001).

[11] E. Eiroa, G. E. Romero and D. F. Torres, Mod. Phys. Lett. A **16**, 973 (2001).

[12] M. Safonova, D. F. Torres and G. E. Romero, Phys. Rev. D **65**, 023001 (2001).

[13] M. Safonova and D. F. Torres, Mod. Phys. Lett. A **17**, 1685 (2002).

[14] K. K. Nandi, Y. Z. Zhang and A. V. Zakharov, Phys. Rev. D **74**, 024020 (2006).

[15] F. Rahaman, M. Kalam and S. Chakraborty, Chin. J. Phys. **45**, 518 (2007).

[16] T. K. Dey and S. Sen, Mod. Phys. Lett. A, **23**, 953 (2008).

[17] N. S. Kardashev, I. D. Novikov and A. A. Shatskiy, Int. J. Mod. Phys. D **16**, 909 (2007).

[18] T. Harko, Z. Kovacs and F. S. N. Lobo, Phys. Rev. D **79**, 064001 (2009).

[19] A. A. Abdujabbarov and B. J. Ahmedov, Astrophys. Space Sci. **321**, 225, (2009).

[20] A. Pozanenko and A. Shatskiy, arXiv:1007.3620[astro-ph.CO].

[21] C. Darwin, Proc. R. Soc. Lond. A **249** (1959).

[22] C. Darwin, Proc. R. Soc. Lond. A **263** (1961).

[23] K. S. Virbhadra and C. R. Keeton, Phys. Rev. D **77**, 124014 (2008).

[24] K. S. Virbhadra, Phys. Rev. D **79**, 083004 (2009).

[25] V. Bozza, Gen. Relativ. Gravit. **42**, 2269 (2010).

[26] V. Bozza and L. Mancini, Astrophys. J. **753**, 56 (2012).

[27] S. Frittelli, T. P. Kling and E. T. Newman, Phys. Rev. D **61**, 064021 (2000).

[28] K. S. Virbhadra and G. F. R. Ellis, Phys. Rev. D **62**, 084003 (2000).

[29] K. S. Virbhadra and G. F. R. Ellis, Phys. Rev. D **65**, 103004 (2002).

[30] V. Bozza, S. Capozziello, G. Iovane and G. Scarpetta, Gen. Relativ. Gravit. **33**, 1535 (2001).

[31] V. Bozza, Phys. Rev. D **66**, 103001 (2002).

[32] W. Hasse and V. Perlick Gen. Relativ. Gravit. **34**, 415 (2001).

[33] V. Perlick, Phys. Rev. D **69**, 064017 (2004).

[34] H. J. Witt and S. Mao, Astrophys. J. **447**, L105 (1995).

[35] S. H. Rhie, Astrophys. J. **484**, 63 (1997).

[36] N. Dalal, Astrophys. J. **509**, L13 (1998).

[37] H. J. Witt and S. Mao, Mon. Not. R. Astron. Soc. **311**, 689 (2000).

[38] N. Dalal and J. M. Rabin, J. Math. Phys. **42**, 1818 (2001).

[39] M. C. Werner, J. Math. Phys. **48**, 052501 (2007).

[40] M. C. Werner, J. Math. Phys. **50**, 082504 (2009).

[41] A. B. Aazami and A. O. Petters, J. Math. Phys. **50**, 032501 (2009).

[42] A. B. Aazami and A. O. Petters, J. Math. Phys. **50**, 082501 (2009).

[43] A. B. Aazami and A. O. Petters, J. Math. Phys. **51**, 023503 (2010).

[44] A. O. Petters and M. C. Werner, Gen. Relativ. Gravit. **42**, 2011 (2010).

[45] A. B. Aazami, A. O. Petters and J. M. Rabin, J. Math. Phys. **52**, 022501 (2011).

[46] A. S. Majumdar and N. Mukherjee, Int. J. Mod. Phys. D **14**, 1095 (2005).

[47] E. Eiroa, Phys. Rev. D **71**, 083010 (2005).

[48] C. R. Keeton and A. O. Petters Phys. Rev. D **73**, 104032 (2006).

[49] P. Schneider, C. S. Kochanek and J. Wambsganss, *Gravitational Lensing: Strong, Weak and Micro, Lecture Notes of the 33rd Saas-Fee Advanced Course*, edited by G. Meylan, P. Jetzer and P. North (Springer-Verlag, Berlin, 2006).

[50] LSST Science Collaborations, arXiv:0912.0201.

[51] R. Takahashi and H. Asada, Astrophys. J. **768**, L16 (2013).

[52] N. Tsukamoto, T. Harada and K. Yajima, Phys. Rev. D **86**, 104062 (2012).

[53] S. Weinberg, *Gravitation and Cosmology: Principles and Applications of the General Theory of Relativity* (Wiley, New York, 1972).

[54] S. Chandrasekhar, *Mathematical Theory of the Black Holes* (Oxford University, New York, 1983).

[55] S. V. Iyer and A. O. Petters Gen. Relativ. Gravit. **39**, 1563 (2007).

[56] P. F. Byrd and M. D. Friedman, *Handbook of Elliptic Integrals for Engineers and Scientists* (Springer-Verlag, New York, 1971).

[57] H. G. Ellis, J. Math. Phys. **14**, 104 (1973).

[58] M. S. Morris and K. S. Thorne, Am. J. Phys. **56**, 395 (1988).

[59] M. S. Morris, K. S. Thorne and U. Yurtsever, Phys. Rev. Lett. **61**, 1446 (1988).

[60] L. Chetouani and G. Clément, Gen. Relativ. Gravit. **16**, 111 (1984).

[61] K. Nakajima and H. Asada, Phys. Rev. D **85**, 107501 (2012).

[62] N. Inada, M. Oguri, M. S. Shin *et al.*, Astron. J. **143**, 119 (2012).

[63] M. Oguri, N. Inada, B. Pindor *et al.*, Astron. J. **132**, 999 (2006).

[64] M. Oguri, N. Inada, M. A. Strauss *et al.*, Astron. J. **135**, 512 (2008).

[65] M. Oguri, N. Inada, M. A. Strauss *et al.*, Astron. J. **143**, 120 (2012).

[66] D. G. York, J. Adelman, J. E. Anderson *et al.*, Astron. J. **120**, 1579 (2000).

[67] A. Barnacka, J.-F. Glicenstein and M. Moderski, Phys. Rev. D **86** 043001 (2012).

[68] C. M. Yoo, T. Harada and N. Tsukamoto, Phys. Rev. D **87** 084045 (2013).

[69] C. Meegan, G. Lichti, P. N. Bhat *et al.*, Astrophys. J. **702**, 791 (2009).

[70] H. Maeda, Phys. Rev. D **79**, 024030 (2009).

[71] T. Harada, H. Maeda and B. J. Carr, Phys. Rev. D **77**, 024022 (2008).

[72] H. Maeda, T. Harada and B. J. Carr, Phys. Rev. D **77**, 024023 (2008).

[73] H. Maeda, T. Harada and B. J. Carr, Phys. Rev. D **79**, 044034 (2009).

[74] B. J. Carr, T. Harada and H. Maeda, Class. Quantum Grav. **27**, 183101 (2010).

[75] J. A. González, F. S. Guzmán and O. Sarbach Class. Quantum Grav. **26**, 015010 (2008).

[76] C. Armendáriz-Picón, Phys. Rev. D **65**, 104010 (2002).

[77] H. Shinkai and S. A. Hayward, Phys. Rev. D **66**, 044005 (2002).

[78] J. A. González, F. S. Guzmán and O. Sarbach Class. Quantum Grav. **26**, 015011 (2008).

[79] A. Doroshkevich, J. Hansen, I. Novikov and A. Shatskiy, Int. J. Mod. Phys. D **18**, 1665 (2009).

[80] F. S. N. Lobo, Phys. Rev. D **71**, 124022 (2005).

[81] L. A. Anchordoqui, D. F. Torres, M. L. Trobo and S. E. Perez Bergliaffa, Phys. Rev. D **57**, 829 (1998).

[82] T. A. Roman, Phys. Rev. D **47**, 1370 (1993).

[83] S. Kar, Phys. Rev. D **49**, 862 (1994).

[84] S. Kar and D. Sahdev, Phys. Rev. D **53**, 722 (1996).

[85] S. Kar, S. SenGupta and S. Sur, Phys. Rev. D **67**, 044005 (2003).

[86] A Das and S. Kar, Class. Quantum Grav. **22**, 3045 (2005).

[87] J. M. Tejeiro and E. A. Larranaga, Rom. J. Phys. **57**, 736 (2012).

[88] F. Abe, Astrophys. J. **725**, 787 (2010).

[89] Y. Toki, T. Kitamura, H. Asada and F. Abe, Astrophys. J. **740**, 121 (2011).

[90] N. Tsukamoto and T. Harada, Phys. Rev. D **87**, 024024 (2013).

[91] E. F. Eiroa and D. F. Torres, Phys. Rev. D **69**, 063004 (2004).

[92] V. Bozza and M. Sereno, Phys. Rev. D **73**, 103004 (2006).

[93] G. S. Bisnovatyi-Kogan and O. Yu. Tsupko, Astrophys. **51**, 99 (2008).

[94] P. Amore and S. Arceo, Phys. Rev. D **73**, 083004 (2006).

[95] P. Amore, M. Cervantes, A. De Pace and F. M. Fernández, Phys. Rev. D **75**, 083005 (2007).

[96] V. Bozza, Phys. Rev. D **67**, 103006 (2003).

[97] V. Bozza, F. De Luca and G. Scarpetta, Phys. Rev. D **74**, 063001 (2006).

[98] V. Bozza, F. De Luca, G. Scarpetta and M. Sereno, Phys. Rev. D **72**, 083003 (2005).

[99] E. F. Eiroa, G. E. Romero and D. F. Torres, Phys. Rev. D **66**, 024010 (2002).

[100] A. Bhadra, Phys. Rev. D **67**, 103009 (2003).

[101] E. Eiroa, Phys. Rev. D **73**, 043002 (2006).

[102] R. Whisker, Phys. Rev. D **71**, 064004 (2005).

[103] E. F. Eiroa and C. M. Sendra Phys. Rev. D **86**, 083009 (2012).

[104] K. Sarkar and A. Bhadra, Class. Quantum Grav. **23**, 6101 (2006).

[105] F. Delplancke, New Astron. Rev. **52**, 199 (2008).

[106] F. Eisenhauer, G. Perrin, W. Brandner *et al.*, Proc. SPIE **7013**, 70132A (2008).

[107] S. Gillessen, F. Eisenhauer, G. Perrin, *et al.*, Proc. SPIE **7734**, 77340Y-20 (2010).

[108] J. U. Pott, J. Woillez, R. L. Akeson, *et al.*, New Astron. Rev. **53**, 363 (2008).

[109] M. Sereno, Phys. Rev. D **69**, 023002 (2004).

[110] M. Sereno and F. De Luca, Phys. Rev. D **74**, 123009 (2006).

[111] F. Delplancke, K. Gorski and A. Richichi, Astron. Astrophys. **375**, 701 (2001).

[112] A. Eckart, T. Bertram, N. Mouawad, T. Viehmann, C. Straubmeier and J. Zuther, Ap&SS, **286**, 269 (2003).

[113] J. P. S. Lemos, F. S. N. Lobo and S. Q. de Oliveira, Phys. Rev. D **68**, 064004 (2003).

[114] N. Kaiser, H. Aussel, B. Burke, *et al.*, Proc. SPIE, **4836**, 154 (2002).

[115] The Dark Energy Survey Collaboration, arXiv:astro-ph/0510346.

[116] S. Miyazaki, Y. Komiyama, H. Nakaya, *et al.*, Proc. SPIE, **6269**, 9 (2006).

[117] T. Kitamura, K. Nakajima and H. Asada, Phys. Rev. D **87**, 027501 (2013).

[118] J. Ebina, T. Osuga, H. Asada and M. Kasai, Prog. Theor. Phys. **104**, 1317 (2000).

[119] B. Paczynski, Astrophys. J. **304**, 1 (1986).